Experimental Fingerprints for Redox-Active Terpyridine in [Cr(tpy)$_2$](PF$_6$)$_n$ (n = 3−0), and the Remarkable Electronic Structure of [Cr(tpy)$_2$]$^{1-}$

Christopher C. Scarborough,[†,‡] Kyle M. Lancaster,[§] Serena DeBeer,[†,§] Thomas Weyhermüller,[†] Stephen Sproules,*[†,‖] and Karl Wieghardt*[†]

[†]Max-Planck-Institut für Bioanorganische Chemie, Stiftstrasse 34-36, D-45470 Mülheim an der Ruhr, Germany

[‡]Department of Chemistry, Emory University, 1515 Dickey Drive, Atlanta Georgia 30322, United States

[§]Department of Chemistry and Chemical Biology, Cornell University, Ithaca, New York 14853, United States

[‖]EPSRC National UK EPR Facility and Service, Photon Science Institute, The University of Manchester, Oxford Road, Manchester M13 9PL, United Kingdom

S *Supporting Information*

ABSTRACT: The molecular and electronic structures of the four members, [Cr(tpy)$_2$](PF$_6$)$_n$ (n = 3−0; complexes **1**−**4**; tpy = 2,2′:6′,2″-terpyridine), of the electron transfer series [Cr-(tpy)$_2$]$^{n+}$ have been determined experimentally by single-crystal X-ray crystallography, by their electro- and magnetochemistry, and by the following spectroscopies: electronic absorption, X-ray absorption (XAS), and electron paramagnetic resonance (EPR). The monoanion of this series, [Cr(tpy)$_2$]$^{1-}$, has been prepared in situ by reduction with KC$_8$ and its EPR spectrum recorded. The structures of **2**, **3**, **4**, **5**, and **6**, where the latter two compounds are the Mo and W analogues of neutral **4**, have been determined at 100(2) K. The optimized geometries of **1**−**6** have been obtained from density functional theoretical (DFT) calculations using the B3LYP functional. The XAS and low-energy region of the electronic spectra have also been calculated using time-dependent (TD)-DFT. A consistent picture of the electronic structures of these octahedral complexes has been established. All one-electron transfer processes on going from **1** to **4** are ligand-based: **1** is [Cr^{III}(tpy^0)$_2$](PF$_6$)$_3$ (S = $^3/_2$), **2** is [Cr^{III}(tpy$^\bullet$)(tpy^0)](PF$_6$)$_2$ (S = 1), **3** is [Cr^{III}(tpy$^\bullet$)$_2$](PF$_6$) (S = $^1/_2$), and **4** is [Cr^{III}(tpy$^{\bullet\bullet}$)(tpy$^\bullet$)]^0 (S = 0), where (tpy^0) is the neutral parent ligand, (tpy$^\bullet$)$^{1-}$ represents its one-electron-reduced π radical monoanion, (tpy^{2-})$^{2-}$ or (tpy$^{\bullet\bullet}$)$^{2-}$ is the corresponding singlet or triplet dianion, and (tpy^{3-})$^{3-}$ (S = $^1/_2$) is the trianion. The electronic structure of **2** cannot be described as [Cr^{II}(tpy^0)$_2$](PF$_6$)$_2$ (a low-spin Cr(II) (d^4; S = 1) complex). The geometrical features (C−C and C−N bond lengths) of these coordinated ligands have been elucidated computationally in the following hypothetical species: [Zn^{II}Cl$_2$(tpy^0)]^0 (S = 0) (**A**), [Zn^{II}(tpy$^\bullet$)Cl(NH$_3$)]^0 (S = $^1/_2$) (**B**), [Zn^{II}(tpy^{2-})(NH$_3$)$_2$]^0 (S = 0 or 1) (**C**), and [Al^{III}(tpy^{3-})(NH$_3$)$_3$]^0 (S = $^1/_2$ and $^3/_2$) (**D**). The remarkable electronic structure of the monoanion has been calculated and experimentally verified by EPR spectroscopy to be [Cr^{III}(tpy^{2-})(tpy$^{\bullet\bullet}$)]$^{1-}$ (S = $^1/_2$), a complex in which the two dianionic tpy ligands differ only in the spin state. It has been clearly established that coordinated tpy ligands are redox-active and can exist in at least four oxidation levels.
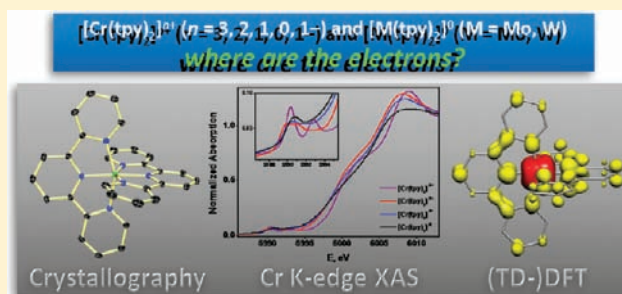
INTRODUCTION

A new entrant into metal-catalyzed alkyl−alkyl cross-coupling chemistry is an organometallic nickel compound bearing a 2,2′:6′,2″-terpyridine (tpy) ligand.[1,2] The catalytically pertinent species is a square planar [Ni(tpy)(alkyl)] that was very recently defined by spectroscopy and density functional theory (DFT) as a central Ni(II) ion coordinated by a π radical monoanion, (tpy$^\bullet$)$^{1-}$.[2,3] This catalytic methodology has since been applied to Negishi-type cross-couplings of C-alkyl and C-aryl glycosides[4,5] and secondary alkylzinc halides with aryl iodides,[6] fluoroalkylation of olefins,[7] and reductive dimerization of alkyl halides, alkyl pseudohalides, and allylic acetates.[8] In each case, a nickel terpyridine complex orchestrates the desired

transformation; the reactivity is tuned by modification of the pincer ligand. This manipulation grants access to different products and chemical outcomes.[4,9] Overall, the salient electronic arrangement is a monoanionic tpy π radical ligand appended to a central Ni ion, wherein the ligand can store and deliver reducing equivalents to the metal ion as required during turnover.[10] It is the unique combination of both electronic (reduction potential) and geometric (meridional coordination) effects inherent to tpy ligands that underscores the success of this Ni-based cross-coupling catalysis, as it was noted that

Table 1. Redox Potentials (V vs Fc$^+$/Fc) for Bis(terpyridine)chromium and Tris(bipyridine)chromium Complexes^a

	3+/2+	2+/1+	1+/0	0/1−	1−/2−	2−/3−	ref
bpy				−2.60	−3.16^b		30
tpy				−2.55	−3.06^b		18
[Cr(bpy)$_3$]^n	−0.63	−1.15	−1.72	−2.34	−2.67	−2.90	26
[Cr(^{t}bpy)$_3$]^n	−0.79	−1.28	−1.81				16
[Cr(tpy)$_2$]^n	−0.53	−0.95	−1.45	−2.37	−2.63 (?)^b	−2.83 (?)^b	26
[Mo(tpy)$_2$]^n	+0.31	−0.72	−1.18				this work
[W(tpy)$_2$]^n	0.00	−0.58	−0.98				this work

^{a}In acetonitrile solutions containing 0.1 M [NEt$_4$](BF$_4$). ^{b}Irreversible.

related N-donor ligands are not as effective or completely ineffective at promoting C−C bond formation.[2,4,9]

In recent years, the role of ligands as simply benign observers in transition-metal-mediated catalysis has been significantly revised.[11] This is best exemplified with systems based on the topologically analogous bis(imino)pyridine (PDI) pincer ligands with earth abundant metals as inexpensive alternatives for catalysis of polymerization, hydrogenation, and aldehyde homologation reactions, their utility attributed to the intrinsic ligand-centered reactivity.[12] Moreover, the potent combination of spectroscopy with theory has provided a clear picture of their intrinsic electronic structure including diagnosis of the metal and ligand redox levels that inevitably improve the catalytic function and efficiency.[13,14]

The reported redox activity of polypyridyl ligands has almost exclusively been confined to the smallest member 2,2′-bipyridine (bpy), chiefly because the neutral species, (bpy^0)^0, and alkali salts of the monoanionic (bpy$^•$)$^{1−}$ and dianionic (bpy$^{2−}$)$^{2−}$ members of this series have been isolated and crystallographically characterized.[15] This structural study established metric parameters with which the oxidation level of the ligand could be diagnosed in coordination compounds,[16,17] the most fruitful being the intrapyridine distance, C_{py}−C'_{py}. Curiously, reduced forms of tpy have almost never been encountered, with only the π radical monoanion detected in a handful of compounds.[2,3,18−20] Nevertheless, the electrochemistry of uncoordinated 2,2′:6′,2″-terpyridine shows successive one-electron reductions:[18] (tpy^0) → (tpy$^•$)$^{1−}$ → (tpy)$^{2−}$ [21] at potentials amazingly similar to those for bpy (Table 1). These reductions involve a sequential filling of the lowest π^* orbital (Figure 1); however, unlike bpy, there is a second π^* orbital to which more electrons can be added such that (tpy$^{3−}$)$^{3−}$ and (tpy$^{4−}$)$^{4−}$ are theoretically conceivable, despite having never been observed to date.[22]

In light of this burgeoning area of chemistry, it seems prudent to explore the redox activity of the archetypical N-
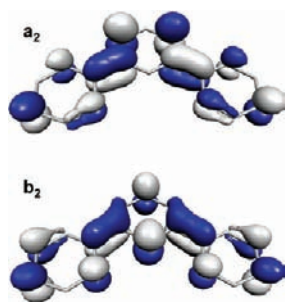
donor pincer ligand, tpy, and establish clear spectroscopic markers diagnostic for the various redox forms of this ligand. To that end, chromium is the ideal metal ion because the bonding is weakly covalent due to the inherent stability of the +III ion resulting from the high exchange energy. We and others have previously exploited this considerably useful attribute with a collection of tris(bidentate) electron transfer series with various N-, O-, and S-donor ligands[16,23−25] and determined that the redox chemistry is entirely ligand-centered leading to Cr(III) complexes with coordinated π-ligand radicals. The five-membered electron transfer series [Cr(tpy)$_2$]^n (n = 3+, 2+, 1+, 0, 1−) is known,[26] and the electrochemistry reveals four reversible one-electron transfer waves and two further irreversible reductions (Table 1). The reduction potentials are strikingly similar to the seven-membered [Cr(bpy)$_3$]^n (n = 3+, 2+, 1+, 0, 1−, 2−, 3−) series.[16,26] The first four members of the tpy series have been isolated and their ground states tentatively established from room temperature magnetic measurements: yellow-brown [Cr(tpy)$_2$]I$_3$·2H$_2$O (S = $^3/_2$); black-blue [Cr(tpy)$_2$]I$_2$·H$_2$O (S = 1); red-brown [Cr(tpy)$_2$]I (S = $^1/_2$); and dark green [Cr(tpy)$_2$] (S = 0).[27] Only [Cr(tpy)$_2$]$^{3+}$ (as the perchlorate salt) has been structurally characterized.[28] The above electrochemical studies show that the monoanionic [Cr(tpy)$_2$]$^{1−}$ species is stable in solution, but no spectroscopic data have been reported.

Herein, we describe the molecular and electronic structures of the members of the electron transfer series [Cr(tpy)$_2$](PF$_6$)$_n$ (n = 3−0) by means of X-ray crystallography, magneto-chemistry, electronic absorption, electron paramagnetic resonance (EPR), X-ray absorption (XAS) spectroscopies, and DFT calculations. We include the monoanion (prepared in situ) and propose a unique electronic structure based on EPR and DFT results. It will be shown that this series is transcended by a central Cr(III) ion with successive reduction of the tpy$_2$ ligand set and thereby debunking the widely accepted notion of [Cr(tpy)$_2$]$^{2+}$ (S = 1) as the prototypical "low-spin" Cr(II) coordination complex as championed in inorganic chemistry textbooks.[29] An electronic absorption band in the near-infrared (NIR) region is seen for the ligand mixed-valent species and assigned as the hallmark intervalence charge transfer (IVCT) band, an accessible fingerprint diagnostic of reduced tpy ligands in homoleptic compounds. This includes experimental and theoretical evidence for the sparingly encountered "excited state" coordination of the triplet dianionic form, (tpy$^{••}$)$^{2−}$, in the neutral and monoanionic members of the series. The proclivity for triplet tpy$^{2−}$ coordination is driven by strong antiferromagnetic coupling with the metal-based SOMOs. For the monoanion, it will be realized that the (t$_{2g}$)^3 electron configuration at the metal limits its ability to stabilize two triplet (tpy)$^{2−}$ ligands. This presents us for the first time with a dizygoleptic (ligands that are nonidentical twins) coordination

Figure 1. Lowest unoccupied molecular orbitals of (tpy^0) with their C_{2v} symmetry designations.

Table 2. Crystallographic Data for 2·2CH₃CN, 3, 4, 5, and 6

	2·2CH$_3$CN	3	4	5	6
chemical formula	C$_{34}$H$_{28}$CrF$_{12}$N$_8$P$_2$	C$_{30}$H$_{22}$CrF$_6$N$_6$P	C$_{30}$H$_{22}$CrN$_6$	C$_{30}$H$_{22}$MoN$_6$	C$_{30}$H$_{22}$N$_6$W
fw	890.58	663.51	518.54	562.48	650.39
space group	$P_4$1, No. 76	$P_2$1/c, No. 14	Fdd2, No. 43	Fdd2, No. 43	Fdd2, No. 43
a, Å	12.3886(14)	8.794(2)	39.443(5)	39.484(6)	39.462(4)
b, Å	12.3886(14)	11.213(2)	56.271(7)	56.962(8)	56.933(5)
c, Å	48.243(6)	27.896(5)	8.3473(11)	8.3177(12)	8.2746(8)
β, deg	90	94.183(3)	90	90	90
V, Å	7404.2(15)	2743.4(9)	18527(4)	18707(5)	18591(3)
Z	8	4	32	32	32
T, K	100(2)	100(2)	100(2)	100(2)	100(2)
ρ(calcd), g cm^{-3}	1.598	1.606	1.487	1.598	1.859
reflns collected/2Θ_{max}	40737/54.98	74293/60.00	219035/66.58	149541/65.00	261189/73.12
unique reflns/$I > 2\sigma(I)$	16282/11735	8003/5944	17806/17170	16940/14174	22686/20054
no. of params/rest.	1089/22	419/342	667/1	667/1	667/1
λ, Å/μ(Kα), cm^{-1}	0.71073/4.95	0.71073/5.50	0.71073/5.28	0.71073/5.95	0.71073/5.05
R1^a/goodness of fit^b	0.0571/1.072	0.0611/1.037	0.0243/1.054	0.0349/1.030	0.0271/1.025
wR2^c ($I > 2\sigma(I)$)	0.0981	0.1731	0.0657	0.0602	0.0501
abs structure param^d	0.01(2)		0.017(5)	0.095(16)	0.031(3)
residual density, e Å^{-3}	+0.51/−0.71	+1.44/−1.17	+0.39/−0.32	+0.48/−0.80	+2.15/−0.97
CCDC depository code	851752	851753	851754	851755	841756

^{a}Observation criterion: $I > 2\sigma(I)$. R1 $= \Sigma||F_o| - |F_c||/\Sigma|F_o|$. ^{b}GoF $= [\Sigma[w(F_o^2 - F_c^2)^2]/(n-p)]^{1/2}$. ^{c}wR2 $= [\Sigma[w(F_o^2 - F_c^2)^2]/\Sigma[w(F_o^2)^2]]^{1/2}$, where $w = 1/\sigma^2(F_o^2) + (aP)^2 + bP$, $P = (F_o^2 + 2F_c^2)/3$. ^{d}Reference 42.

complex, where the two ligands differ *only* in spin state, one a singlet (tpy^{2-})$^{2-}$ and the other a triplet (tpy$^{••}$)$^{2-}$. In addition, we characterize the complexes [M(tpy)$_2$]^0 (M = Mo (**5**), W (**6**)) by X-ray crystallography and electronic spectroscopy, where the increased effective nuclear charge of the metal ion generates even more reduced tpy$_2$ ligand sets that formally involve contributions from the (tpy^{3-})$^{3-}$ level.

■ EXPERIMENTAL SECTION

1.1. Synthesis of Compounds. The following syntheses were carried out using standard Schlenk techniques or a glovebox in the absence of water and dioxygen unless stated otherwise. The ligand 2,2′:6′,2″-terpyridine (Sigma-Aldrich), AgPF$_6$ (Sigma-Aldrich), NH$_4$PF$_6$ (Sigma-Aldrich), anhydrous CrCl$_2$ (Strem), and M(CO)$_6$ (M = Cr, Mo, W) (Sigma-Aldrich) are commercially available.

[Cr(tpy)$_2$](PF$_6$)$_3$ (1). Red-brown **2** (100 mg; 0.12 mmol) was dissolved in 2 mL of CH$_3$CN. Separately, AgPF$_6$ (30 mg; 0.12 mmol) was dissolved in 1 mL of CH$_3$CN, and this solution was added over 20 s to the stirred solution of **2** affording a brown suspension. After 15 min, the CH$_3$CN was removed under vacuum to afford a brown residue. The product was reconstituted in CH$_3$CN and filtered through Celite, and the solvent was removed under vacuum. The residue was triturated, then washed with THF, and dried under vacuum to give orange **1**. Yield: 85 mg (72%). Diffraction-quality crystals were obtained by vapor diffusion of Et$_2$O into a concentrated CH$_3$CN solution.

Anal. Calcd for C$_{30}$H$_{22}$N$_6$CrP$_3$F$_{18}$: C, 37.79; H, 2.32; N, 8.81; Cr, 5.45; P, 9.74. Found: C, 38.34; H, 2.67; N, 9.57; Cr, 5.25; P, 9.32.

[Cr(tpy)$_2$](PF$_6$)$_2$ (2). To 30 mL of degassed water in a 50 mL Schlenk flask was added 2,2′:6′,2″-terpyridine (510 mg; 2.19 mmol) and CrCl$_2$ (135 mg; 1.10 mmol). The solution was stirred at room temperature for 20 h, during which time the color transitioned from light blue to dark brown. A degassed aqueous solution of NH$_4$PF$_6$ (5 mL; 0.44 M; 2.20 mmol) was added, resulting in precipitation of **2**. The suspension was filtered through a Schlenk frit, and the solid was washed with 50 mL of degassed water. The solid was dried under vacuum, reconstituted in dry CH$_3$CN, and filtered. The solvent was stripped affording microcrystalline **2**. Yield: 785 mg (89%). Diffraction-quality crystals of were grown by vapor diffusion of Et$_2$O into a concentrated solution in CH$_3$CN.

Anal. Calcd for C$_{30}$H$_{22}$N$_6$CrP$_2$F$_{12}$: C, 44.57; H, 2.74; N, 10.39; Cr, 6.43; P, 7.66. Found: C, 44.89; H, 2.78; N, 11.02; Cr, 6.22; P 7.53.

[Cr(tpy)$_2$](PF$_6$) (3). A solution of AgPF$_6$ (24 mg; 0.10 mmol) in THF (2 mL) was added dropwise to a dark green solution of **4** (50 mg; 0.10 mmol) in THF (5 mL). The mixture immediately became red-brown. After stirring for 30 min, the solvent was removed and the solid residue was taken up in CH$_3$CN and filtered through Celite. Removal of the CH$_3$CN under vacuum afforded **3**. Yield: 67 mg (94%). Diffraction-quality crystals were grown by vapor diffusion of Et$_2$O into a concentrated CH$_3$CN solution.

Anal. Calcd for C$_{30}$H$_{22}$N$_6$CrPF$_6$: C, 54.31; H, 3.34; N, 12.67; Cr, 7.84; P, 4.67. Found: C, 54.23; H, 3.67; N, 12.44; Cr, 7.77; P, 4.61.

[Cr(tpy)$_2$] (4). A 100 mL Schlenk flask was charged with Cr(CO)$_6$ (249 mg; 1.13 mmol) and 2,2′:6′,2″-terpyridine (525 mg; 2.25 mmol) dissolved in mesitylene (55 mL). The flask was fitted with a reflux condenser and purged with argon, and the solution was refluxed for 6 h. A crystalline solid formed upon gradual cooling of the reaction mixture to room temperature that was collected by filtration and washed with 20 mL of dry, deoxygenated Et$_2$O. The resultant black, diffraction-quality crystals were dried under vacuum. Yield: 334 mg (29%).

Anal. Calcd for C$_{30}$H$_{22}$N$_6$Cr: C, 69.49; H, 4.28; N, 16.21; Cr, 10.03. Found: C, 68.97; H, 4.34; N, 15.95; Cr, 10.00.

[Mo(tpy)$_2$] (5). To a 100 mL Schlenk flask was added Mo(CO)$_6$ (99 mg; 0.37 mmol), tpy (175 mg; 0.75 mmol), and *n*-pentadecane (20 mL). The flask was fitted with a condenser, purged with argon, and heated to reflux for 5 h. After slowly cooling to room temperature, the crystalline solid was collected on a Schlenk frit under argon. The resultant dark purple, diffraction-quality crystals were dried under vacuum. Yield: 167 mg (79%). Properties match those reported previously for this compound.[31]

[W(tpy)$_2$] (6). A 20 mL amount of a *n*-pentadecane solution of W(CO)$_6$ (352 mg; 1.0 mmol) and tpy (420 mg; 1.8 mmol) in a 100 mL Schlenk flask fitted with a condenser was refluxed for 5 h under argon. The reaction mixture was slowly cooled to room temperature, inducing precipitation of a crystalline solid that was collected on a Schlenk frit under argon. The resultant dark green, diffraction-quality crystals were dried in vacuo. Yield: 534 mg (82%). This compound has been previously characterized.[31]

1.2. Physical Methods. Electronic absorption spectra were obtained on a Perkin-Elmer Lambda 19 double-beam UV/vis/NIR

spectrometer (300−2000 nm). Infrared spectra were measured on a Perkin-Elmer System 2000 FT-IR spectrometer (450−7800 cm^{-1}) as pressed KBr discs. Cyclic voltammograms were recorded with an EG&G potentiostat/galvanostat 273A. A three-electrode cell was employed with a glassy carbon working electrode, a glassy carbon auxiliary electrode, and a Ag/AgNO$_3$ reference electrode (0.01 M AgNO$_3$ in CH$_3$CN) in dichloromethane solution containing 0.1 M [N(n-Bu)$_4$](PF$_6$) as supporting electrolyte. Ferrocene was added as an internal standard after completion of the measurements, and potentials are referenced versus the Fc$^+$/Fc couple. Variable-temperature (4−290 K) magnetization data were recorded in a 1 T magnetic field on a SQUID magnetometer (MPMS Quantum Design). Experimental magnetic susceptibility data were corrected for underlying diamagnetism using tabulated Pascal's constants. X-band EPR spectra were recorded on a Bruker ELEXSYS E500 spectrometer, whereas S-band spectra were obtained on a Bruker ESP 300E spectrometer. Spectral manipulation and simulation were performed with the Bruker XSOPHE suite.[32] Cr K-edge XAS data were measured at the Stanford Synchrotron Radiation Lightsource (SSRL) under ring conditions of 3.0 GeV and 300 mA. Data were measured on beamline 7-3 as previously described.[23,25,33] Elemental analyses were performed by H. Kolbe at the Mikroanalytischen Labor in Mülheim an der Ruhr, Germany.

1.3. Calculations. All DFT calculations were performed with the ORCA program package.[34] Complexes were geometry optimized using the B3LYP functional.[35] Electronic structure and absorption (electronic and X-ray) TD-DFT calculations were carried out as described in detail in ref 16 except for the following three improvements: (1) here we included an empirical van der Waals correction to the DFT energy,[36] (2) for complexes **5** and **6**, which contain a second- and a third-row transition metal ion, respectively, we implemented the zeroth-order regular approximation (ZORA) method[37] and the associated basis set ZORA-TZVP[38] for the metal center, and (3) the radial integration accuracy for all calculations was elevated to 10 for the transition metal (Cr, Mo, or W) and 5 for all other atoms.

1.4. X-ray Crystallographic Data Collection and Refinement of the Structures. Single crystals of complexes **2·2CH$_3$CN, 3, 4, 5,** and **6** were coated with perfluoropolyether, picked up with nylon loops, and immediately mounted in the nitrogen cold stream of the diffractometer. Graphite-monochromated Mo Kα radiation (λ = 0.71073 Å) from a Mo-target rotating-anode X-ray source was used throughout. Final cell constants were obtained from least-squares fits of several thousand strong reflections. Intensity data were corrected for absorption using intensities of redundant reflections with the program SADABS.[39] Structures were readily solved by Patterson methods and subsequent difference Fourier techniques. The Siemens ShelXTL[40] software package was used for solution and artwork of the structures, and ShelXL97[41] was used for the refinement. All non-hydrogen atoms were anisotropically refined, and hydrogen atoms were placed at calculated positions and refined as riding atoms with isotropic displacement parameters. Crystallographic data of the compounds are listed in Table 2. One of the four crystallographically independent PF$_6^-$ ions in the asymmetric unit of **2·2CH$_3$CN** was found to be disordered. A split atom model was refined yielding an occupation factor ratio of about 0.7:0.3. EADP and SAME instructions of ShelXL97[41] were used to restrain bond distances and thermal displacement parameters of split parts. A similar problem occurred in crystals of **3**. The occupation ratio was found to be about 0.9:0.1 in this case. EADP and SADI restraints were used.

■ **RESULTS**

2.1. Synthesis and Characterization of Complexes. In 1966, Herzog and Aul[27] reported the synthesis of [Cr(tpy)$_2$]-I$_2$·H$_2$O as blue-black crystals from a solution of CrI$_2$ in HI by addition of the ligand tpy (2:1) dissolved in ethanol. Oxidation of this species by I$_2$ in H$_2$O affords yellow-brown [Cr(tpy)$_2$]-I$_3$·2H$_2$O. Red [Cr(tpy)$_2$]I was obtained via disproportionation of the dication in alkaline solution. Finally, they reported that

the green neutral species [Cr(tpy)$_2$] was obtained via reduction of the dication in DMF with Mg. Behrens and Anders reported the synthesis of the neutral species via ligand exchange reactions of [Cr^0(benzene)$_2$], [Cr^0(CO)$_6$], or [Cr^0(CN)$_6$]$^{6-}$ with 2 equiv of tpy. Similarly, the neutral complexes [Mo(tpy)$_2$] (**5**) and [W(tpy)$_2$] (**6**) were synthesized from M(CO)$_6$ (M = Mo, W) and 2 equiv of tpy at 180 °C.[31,43] From room temperature magnetic measurements[27] it was established that the dication possesses an S = 1 ground state (μ$_{eff}$ = 2.80 μ$_B$), the monocation possesses an S = $^1/_2$ ground state (μ$_{eff}$ = 1.85 μ$_B$), and all three neutral species (**4−6**) were reported to be diamagnetic.[27,31]

Here, we synthesized the neutral complexes **4, 5,** and **6** from the corresponding hexacarbonyl starting material M(CO)$_6$ (M = Cr, Mo, W) and 2 equiv of tpy in refluxing mesitylene (M = Cr) or n-pentadecane (M = Mo, W) under an argon-blanketed atmosphere. We also synthesized the hexafluorophosphate salts **1, 2,** and **3** (Chart 1). Oxidation of dark green **4** by 1 equiv of

Chart 1. Complexes

[Cr^{III}(tpy^0)$_2$](PF$_6$)$_3$	(S = 3/2)	**1**
[Cr^{III}(tpy$^•$)(tpy^0)](PF$_6$)$_2$	(S = 1)	**2**
[Cr^{III}(tpy$^•$)$_2$](PF$_6$)	(S = 1/2)	**3**
[Cr^{III}(tpy$^{••}$)(tpy$^•$)]^0	(S = 0)	**4**
[Mo(tpy)$_2$]^0	(S = 0)	**5**
[W(tpy)$_2$]^0	(S = 0)	**6**

AgPF$_6$ in THF produces red-brown **3**. Reaction of CrCl$_2$ in water under an argon atmosphere with 2 equiv of tpy afforded, after addition of excess NH$_4$PF$_6$, complex **2**. Finally, oxidation of **2** by 1 equiv of AgPF$_6$ in acetonitrile generated orange **1**. Complexes **2−6** have been obtained as single crystals suitable for X-ray diffraction analysis (vide infra).

The temperature dependence of the magnetic susceptibility of complexes **1−6** has been studied in the range 4−290 K using a SQUID magnetometer (1 T external magnetic field), and these data are displayed in Figure S1, Supporting Information. **1** displays a temperature-independent (10−290 K) magnetic moment of 3.92 μ$_B$ (S = $^3/_2$) in agreement with its EPR spectrum,[44] **2** exhibits a temperature-independent (10−290 K) magnetic moment of 2.74 μ$_B$ (S = 1) and **3** a magnetic moment of 1.78 μ$_B$ (S = $^1/_2$). Neutral complexes **4, 5,** and **6** are all diamagnetic.

X-band (∼9.5 GHz) EPR spectra of **3** (S = $^1/_2$) have been recorded in a CH$_2$Cl$_2$/THF solution at 20 and 200 K. The near axial frozen solution spectrum shown in Figure 2 has pronounced anisotropy of the principal g-values, g = (2.0537, 2.0471, 1.9603). Satellite lines due to hyperfine coupling to the ^{53}Cr (I = $^3/_2$, 9.53% natural abundance) isotope are faintly visible on the lowest g-value and clearly buried in the intrinsic field-dependent line width of higher ones. The inherently broad fluid solution spectrum obscured the isotropic ^{53}Cr hyperfine features and precluded an estimate of A$_⊥$ (Figure S2, Supporting Information). A lower frequency measurement at the S-band (∼3.7 GHz) revealed an axial hyperfine splitting, and simulation gave A = (−20, −20, −29) × 10^{-4} cm^{-1} (Figure S3, Supporting Information). The fluid solution spectrum at the S-band failed to reveal isotropic ^{53}Cr hyperfine coupling (Figure S4, Supporting Information); however, both the S- and the X-band chilled solution spectra (200 K) have the same peak-to-peak separation, which indicates that the inhomogeneous line broadening is a consequence of unresolved ^{14}N (I =
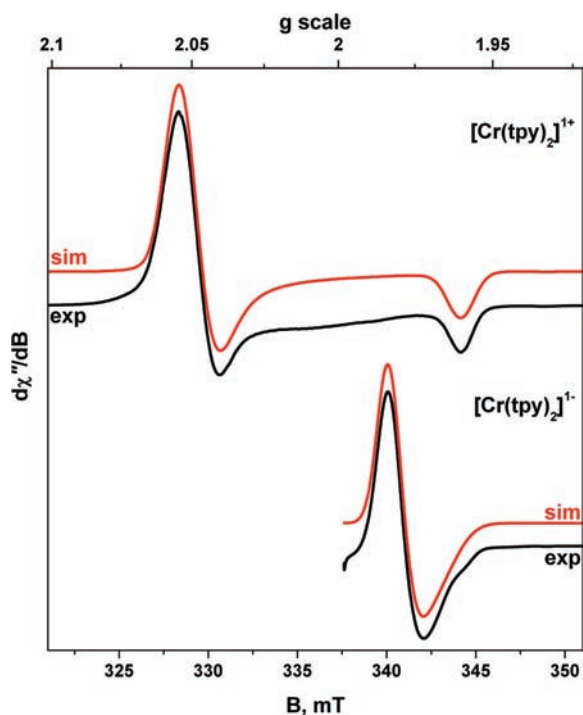
Figure 2. (Top) X-band EPR spectra of **3** recorded in CH_2Cl_2/THF solution at 20 K (conditions: frequency 9.4418 GHz; power 0.02 mW; modulation 0.8 mT). (Bottom) X-band EPR spectra of $[Cr(tpy)_2]^{1-}$ recorded in THF solution at 30 K (conditions: frequency 9.6574 GHz; power 0.63 mW; modulation 0.2 mT). Experimental data are depicted by the black trace. Simulations are shown in red, and parameters are given in the text.

1, 99.63% natural abundance) hyperfine coupling that is estimated to be $\sim 3 \times 10^{-4}$ cm^{-1}. These spectra are in stark contrast to the fluid solution spectrum of $[Cr^{III}(^tbpy^{\bullet})_2(^tbpy)]^{1+}$ ($S = 1/2$), where ^tbpy represents 4,4'-di-*tert*-butyl-2,2'-bipyridine, reported previously, where $g_{iso} = 1.9973$, $A\{^{53}Cr\} = 21.8 \times 10^{-4}$ cm^{-1}, and, most notably, a rich multiline splitting due to $A\{^{14}N\} = 3.05 \times 10^{-4}$ cm^{-1}.[16] Although we can estimate similar ^{14}N coupling constants for both compounds, the lack of resolvable hyperfine structure in **3** plausibly stems from slow tumbling in solution brought about the relatively exposed ligand planes to anisotropic solvent interactions or the nearby positioning of the PF_6^- counterion where broadening arises from a weak ^{19}F hyperfine interaction. The substantial ^{53}Cr hyperfine interaction in **3** is of similar magnitude to $[Cr^{III}(^tbpy^{\bullet})_2(^tbpy)]^{1+}$ and indicates that the unpaired electron resides in a Cr d orbital. However, the large g-anisotropy in **3** arises from the different singly occupied molecular orbital (SOMO) for bis(terdentate) and tris-(bidentate) complexes, that being b_1 (d_{xy}) in D_{2d} symmetric **3** compared to a_1 (d_{z^2}) in D_3-symmetric $[Cr^{III}(^tbpy^{\bullet})_2(^tbpy)]^{1+}$, and indicates a smaller splitting of the three metal-based SOMOs in **3** than for the latter. The appearance of low-energy electronic transitions in **3** support this interpretation (vide infra). As we will demonstrate, the doublet ground state of **3** is attained via strong intramolecular antiferromagnetic coupling between the spins of three unpaired electrons of a central Cr(III) ion with $(t_{2g})^3$ configuration and two π radical monoanions $(tpy^{\bullet})^{1-}$; the net spin resides on the Cr ion.

The monoanionic member of the series $[Cr(tpy)_2]^{1-}$ was prepared in situ by treating a THF solution of **4** with potassium graphite (KC_8) in an EPR tube. The spectrum recorded at 30 K

is consistent with a doublet ground state ($S = 1/2$) with a weakly axial signal centered on $g \approx 1.97$ (Figure 2). The same spectrum also carried a sharp feature at $g = 2.005$ due to paramagnetic KC_8 suspended in the frozen THF matrix (Figure S5, Supporting Information), as verified by an independent measurement of the reducing agent (Figure S6, Supporting Information). Spectral simulation yielded $g = (1.9835, 1.9783, 1.9683)$, and no hyperfine splitting was observed. The high-field shoulder was difficult to include in the simulation; it lacks sufficient intensity to be the lowest g-value and probably arises from hyperfine coupling of ^{53}Cr, ^{14}N, and ^{1}H nuclei not sufficiently resolved at this frequency. The fluid solution spectrum exhibited an extraordinarily broad signal with $g_{iso} = 1.9735$ dissected by the sharp resonance from excess KC_8 (Figure S7, Supporting Information). These g values clearly establish a Cr-based paramagnet for $[Cr(tpy)_2]^{1-}$ despite the lack of g-anisotropy, in contrast to **3**, which is conceivably attenuated by the reduced metal content of the SOMO and lowering of symmetry as described by DFT calculations (vide infra). Exposing this sample to air leads to a loss of both the KC_8 and the $[Cr(tpy)_2]^{1-}$ signals, introducing a small isotropic resonance at $g \approx 2.01$, presumably free $(tpy^{\bullet})^{1-}$, and the highly anisotropic profile of **3**, thus confirming that the $\{Cr(tpy)_2\}$ unit is conserved during the in situ reduction and moreover that the $g \approx 1.97$ signal belongs to the monoanion. Therefore, this compound has the truly exceptional electronic structure $[Cr^{III}(tpy^{2-})(tpy^{\bullet\bullet})]^{1-}$, the first example of a dizygoleptic coordination complex that binds two ligands differing only in their spin state: one diamagnetic (tpy^{2-}) ($S_L = 0$) ligand and one triplet $(tpy^{\bullet\bullet})^{2-}$ ($S_L = 1$) ligand bound to the central Cr(III) (d^3; $S_{Cr} = 3/2$) ion to leave net spin on the metal.

The electronic absorption spectra of compounds **1−6** in acetonitrile, THF, or CH_2Cl_2 solution are presented in Figure 3; the transitions are summarized in Table 3. The electronic spectra of Li(tpy$^{\bullet}$) and $[Fe^{II}(tpy)_2]^{2+,1+,0}$ have been reported.[45,46] For $(tpy^{\bullet})^{1-}$, intense ($\sim 10^4$ M^{-1} cm^{-1}) bands have been observed at 30 000−25 000, 22 220 (sh), 16 130, 14 200, and 10 640 cm^{-1} that are speculatively identified as $\pi \rightarrow \pi^*$ and $\pi^* \rightarrow \pi^*$ transitions.[45] These peaks are also observed in the spectra of $[Fe^{II}(tpy^{\bullet})(tpy^0)]^{1+}$ and $[Fe^{II}(tpy^{\bullet})_2]^0$ and in complexes **2**, **3**, and **4**. The latter three exhibit three prominent bands in the visible region (**2**: 25 810, 20 080, and 17 860 cm^{-1}; **3**: 23 000, 17 150, and 13 970 cm^{-1}; **4**: 22 620, 15 950, and 13 050 cm^{-1}) assigned as $\pi^* \rightarrow \pi^*$ transitions of the $(tpy^{\bullet})^{1-}$ ligand present in each. An additional cluster of low-energy transitions around 10 000 cm^{-1} in the spectra of **2** and **3** is similarly ascribed. A similar profile, though profoundly more intense, is witnessed in the spectrum of **4** centered at 7500 cm^{-1}, which may be attributed to ligand-to-ligand charge transfer (LLCT) between the mixed-valent tpy ligands, one $(tpy^{\bullet})^{1-}$ and one $(tpy^{\bullet\bullet})^{2-}$, with the aid of time-dependent (TD)-DFT calculations (vide infra). More detailed assignments cannot be provided at this point as the spectrum of uncoordinated $(tpy^{\bullet\bullet})^{2-}$ is not known. The spectral profile of **5** and **6** are contrasted with **4** in the lower panel of Figure 3 and clearly indicate the presence of reduced tpy ligands in these neutral complexes.

Interestingly, the spectrum of **2** exhibits an additional low-energy electronic transition at 2700 cm^{-1} in the IR region (vide infra). We tentatively assign this band as the intervalence charge transfer (IVCT) transition occurring from the $(tpy^{\bullet})^{1-}$ ligand into the bonding combination of the two tpy LUMO+1 fragment orbitals, an assignment that we corroborated with
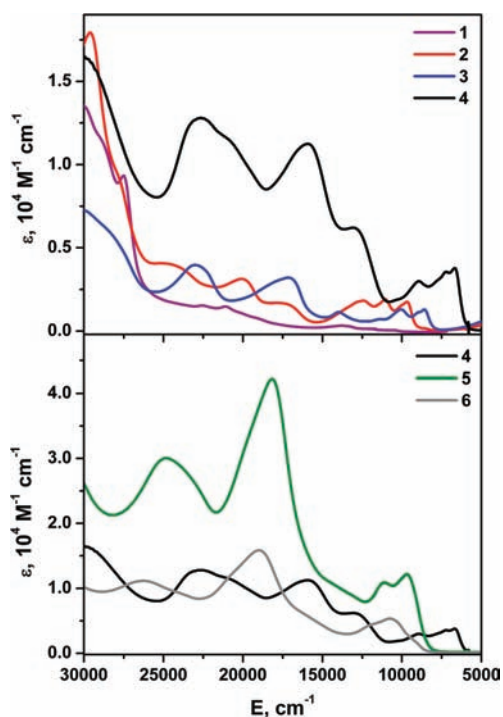
Figure 3. (Top) Electronic absorption spectra of **1−3** in CH₃CN and **4** in THF at ambient temperature. (Bottom) Electronic spectra of **4−6** in CH₂Cl₂ at ambient temperature.

Table 3. Experimental and Calculated Electronic Transition Energies (cm^{-1}) for Complexes[a]

complex	obsd	calcd	assignment[b]
2	n.o.	522	IVCT
	2700 (br)	3213	LLCT
	9680	8664	
	10 000 (sh)	n.c.	$\pi^* \to \pi^*$ (tpy$^\bullet$)$^{1-}$
	11 050		
	12 420		
	17 860 (sh)		
	20 080		
	25 810		
3	4500	4507	LLCT
	5500	4513	
	8570	9085	
	8930	9089	
	11 325	n.c.	$\pi^* \to \pi^*$ (tpy$^\bullet$)$^{1-}$
	13 970		
	17 150		
	18 200		
	23 000		
4	6680	6422	IVCT
	7210	7120	LLCT
		7127	
	8930	n.c.	$\pi^* \to \pi^*$ (tpy$^\bullet$)$^{1-}$
	13 050		
	15 950		
	21 000 (sh)		
	22 620		
Li(tpy$^\bullet$)[c]	10 530	n.c.	$\pi^* \to \pi^*$ (tpy$^\bullet$)$^{1-}$
	14 850		
	16 130		
	16 800		
	23 800		
	25 600		

[a]Abbreviations: n.o. = not observed, n.c. = not calculated; br = broad, sh = shoulder, IVCT = intervalence charge transfer, LLCT = ligand-to-ligand charge transfer. [b]Details of these transitions are given in the text. [c]Reference 45.

TD-DFT calculations (vide infra). This transition has also been reported for $[\mathrm{Ru^{II}(bpy^\bullet)_2(bpy^0)}]^0$ at 4000 cm^{-1} and assigned to the (bpy$^\bullet$)$^{1-}$/(bpy^0) IVCT transition.[47] Moreover, this band is seen in the spectrum of **4** at 6680 cm^{-1} but notably absent in the corresponding spectrum of $[\mathrm{Cr^{III}(bpy^\bullet)_3}]^0$.[16]

The most salient feature of the electronic spectra of **2** is the observation of numerous transitions (25 000−4000 cm^{-1}) with intensities $\varepsilon > 100$ M^{-1} cm^{-1} that are incongruous with a $[\mathrm{Cr^{II}(tpy^0)_2}]^{2+}$ electronic structure description.[29]

X-ray Crystal Structures. We determined the crystal structures of complexes **2−6**. Data were collected at cryogenic temperature (100(2) K). Table 4 summarizes selected bond distances of the {M(tpy)} units.

The structures of $[\mathrm{Cr^{III}(tpy^0)_2}](\mathrm{ClO_4})_3 \cdot \mathrm{H_2O}$ and $[\mathrm{Cr^{III}(tpy^0)Cl_3}] \cdot \mathrm{DMSO}$ have been reported.[28] These two structures represent benchmarks for the structural details of a terdentate, neutral (tpy^0) ligand coordinated to a Cr(III) ion in a distorted octahedral environment. From these data, we establish the characteristic C−C and C−N bond distances of a {Cr^{III}(tpy^0)} unit. The most important features are (a) the presence of two equivalent C_{py}−C'_{py} bonds at 1.48 ± 0.01 Å that are characteristic of C−C single bonds between two sp²-hybridized carbon atoms, (b) the other average C−C and C−N bond lengths at 1.38 ± 0.01 and 1.35 ± 0.01 Å, respectively, which are typical for aromatic pyridine rings, and (c) the Cr−N bonds of the terminal two pyridine rings of (tpy^0) are longer (at 2.06 ± 0.01 Å) than the corresponding Cr−N bond of the central pyridine ring (at 1.98 ± 0.01 Å).

The crystal structure of $[\mathrm{Cr(tpy)_2}](\mathrm{PF_6})_2 \cdot 2\mathrm{CH_3CN}$ (**2**) is remarkable in that the two tpy ligands are not equivalent. One neutral (tpy^0) ligand is characterized with C−N, C_{py}−C'_{py}, and Cr−N bond distances as shown above for the trication $[\mathrm{Cr^{III}(tpy^0)_2}]^{3+}$ and neutral $[\mathrm{Cr^{III}(tpy)Cl_3}]^0$ (Table 4); the other coordinated ligand is clearly a (tpy$^\bullet$)$^{1-}$ π radical

monoanion:[1,20,49,50] the two C_{py}−C'_{py} bonds at 1.45 ± 0.02 Å are shorter than in {Cr^{III}(tpy^0)} units, and the C−N bonds of the central pyridine ring are longer at 1.38 ± 0.02 Å, whereas the C−N bonds of the terminal pyridine ring at an average of 1.365 ± 0.02 Å are only slightly longer than those in (tpy^0). The Cr−N bonds of the neutral (tpy^0) and π radical monoanion (tpy$^\bullet$)$^{1-}$ also differ significantly: the central Cr−N bond in the {Cr^{III}(tpy^0)} unit is longer than that in the {Cr^{III}(tpy$^\bullet$)} unit by 0.08 Å. In contrast, the two terminal Cr−N bonds in the {Cr^{III}(tpy^0)} unit at 2.064 ± 0.01 Å and those in the {Cr^{III}(tpy$^\bullet$)} unit at 2.042 ± 0.01 Å differ only slightly. These structural data are incompatible with the description of **2** as $[\mathrm{Cr^{II}(tpy^0)_2}](\mathrm{PF_6})_2$.[29] The correct electronic structure is best described as $[\mathrm{Cr^{III}(tpy^\bullet)(tpy^0)}](\mathrm{PF_6})_2$. We emphasize that, at least in the solid state, the coordinated π radical anion (tpy$^\bullet$)$^{1-}$ is localized, as found in $[\mathrm{Cr^{III}(^tbpy^\bullet)(^tbpy^0)_2}](\mathrm{PF_6})_2$,[16] which is also not a low-spin Cr(II) species.

The structure of the monocation in **3** displays two equivalent coordinated (tpy$^\bullet$)$^{1-}$ π radicals. The C_{py}−C'_{py} bonds are shorter and the C−N bonds longer than those in coordinated (tpy^0), and most significantly, the two Cr−N bonds to the central (reduced) pyridine rings of (tpy$^\bullet$)$^{1-}$ are much shorter

3723

dx.doi.org/10.1021/ic2027219 | *Inorg. Chem.* 2012, 51, 3718−3732

Table 4. Selected Averaged Experimental Bond Distances (Å) of Complexes

complex	M−N_C	M−N_t	C_{py}−C'_{py}	N_t−C'_{py}	N_t−C'	N_c−C_{py}	oxidation level
$[Cr^{III}(tpy^0)Cl_3]^a$	1.992(2)	2.074(2)	1.478(2)	1.362(2)	1.341(2)	1.345(2)	1 (tpy^0)
$[Cr^{III}(tpy^0)_2]^{3+ b}$	1.976(5)	2.056(5)	1.472(9)	1.360(9)	1.344(9)	1.364(9)	2 (tpy^0)
2	1.916(4)	2.042(4)	1.448(7)	1.379(6)	1.351(6)	1.378(6)	$(tpy^•)^{1−}$
	1.997(4)	2.064(4)	1.482(6)	1.365(6)	1.345(6)	1.350(5)	(tpy^0)
3	1.928(2)	2.047(3)	1.448(5)	1.369(6)	1.355(4)	1.381(5)	2 $(tpy^•)^{1−}$
4	1.949(1)	2.018(1)	1.439(2)	1.380(1)	1.362(1)	1.387(1)	$(tpy^•)^{1−}$, $(tpy^{••})^{2−}$
5	2.034(2)	2.101(2)	1.433(4)	1.386(3)	1.367(3)	1.394(3)	$(tpy_2)^{4−}$
6	2.050(2)	2.077(2)	1.422(4)	1.388(3)	1.374(3)	1.400(3)	$(tpy_2)^{5−}$

^{a}Reference 48. ^{b}Reference 28.

than those in the $\{Cr^{III}(tpy^0)\}$ units in **1**. Therefore, the electronic structure of the monocation in **3** is best described as $[Cr^{III}(tpy^•)_2]^{1+}$.

The structure of the diamagnetic neutral complex [Cr-$(tpy)_2]^0$ (**4**) shown in Figure 4 displays two equivalent, reduced
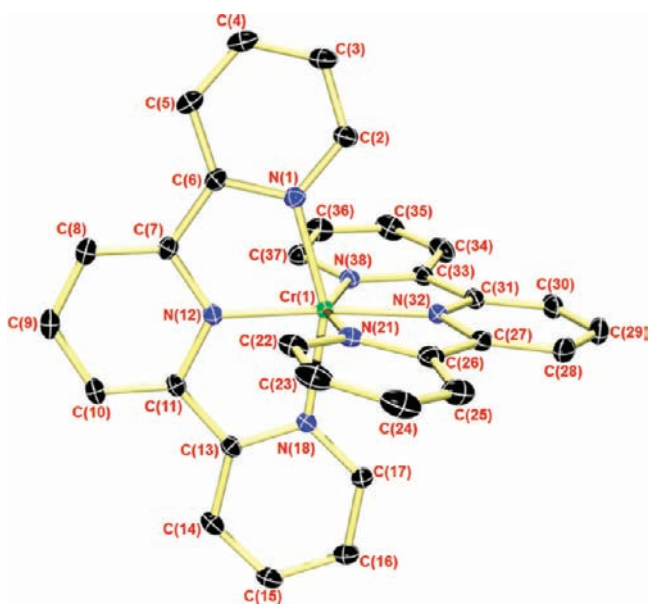
Figure 4. Structure of the neutral complex in crystals of **4** (50% probability). Structures of neutral **5** and **6** and those of the cations in **2** and **3** are very similar and available in the Supporting Information. Hydrogen atoms omitted for clarity.

tpy ligands. The average short C_{py}−C'_{py} bond length of 1.440(2) Å and the elongated C−N bonds at the central and terminal pyridine rings, in comparison to those in $(tpy^•)^{1−}$, indicate an oxidation level of the two tpy ligands that is more reduced than in the localized $(tpy^•)^{1−}$ π radical monoanion (Table 4). Since we will show below that the central chromium ion in **4** possesses a +III oxidation state $(d^3, S_{Cr} = {}^3/_2)$, we propose here that the observed structural parameters of the two equivalent tpy ligands imply the presence of one $(tpy^•)^{1−}$ and one $(tpy^{••})^{2−}$, where the excess electron is delocalized over both tpy ligands, i.e., an $S = {}^3/_2$ $(tpy_2)^{3−}$ unit.

These structural data on complexes **1−4** suggest that the oxidation state of the central chromium ion remains constant at +III throughout the series: reduction of **1** by one, two, and

three electrons is ligand-based. This is concomitant with a monotonic decrease in the average C_{py}−C'_{py} distance with decreasing charge as described in Figure 5. This is a
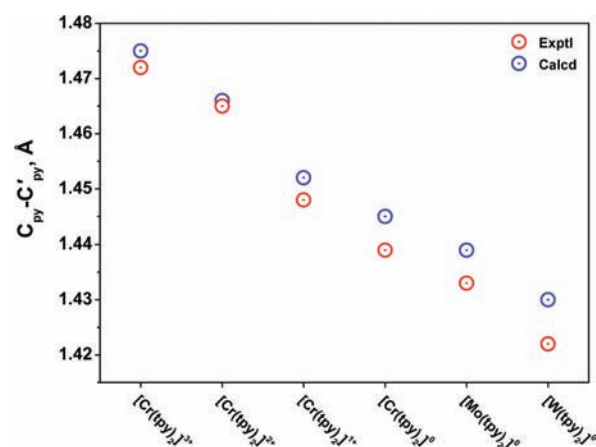

Figure 5. Plot of the experimentally averaged C_{py}−C'_{py} bond distances (Å) of the two tpy ligands in **1−6** (red) and the corresponding calculated values (blue) from DFT calculations.

consequence of filling the LUMO and LUMO+1 of two (tpy^0) ligands with zero, one, two, or three electrons (Figure 1).

It is worth noting that the neutral complexes **5** and **6** containing heavier transition metal ions crystallize in the same space group as **4** (Table 2) with two crystallographically independent molecules per asymmetric unit. These two molecules are identical within the 3σ limits. Interestingly, the C_{py}−C'_{py}, C−C, and C−N bond distances in **4**, **5**, and **6** are not identical: the C_{py}−C'_{py} bond length decreases in the order Cr > Mo > W (Figure 5), and the C−N bond distances increase in that order. With experimental verification for a Cr(III) central ion in **4** (vide infra), and therefore a $(tpy_2)^{3−}$ ligand unit, the progressive shortening of the C_{py}−C'_{py} bond from across this series is suggestive of a $(tpy_2)^{4−}$ moiety in **5** and $(tpy_2)^{5−}$ in **6**. This implies Mo(IV) and W(V) central ions for charge balance, though this assignment is strictly tentative given the pervasive covalency in **5** and **6**.

Cr K-Edge XAS. The effective nuclear charge (oxidation state) of the central chromium ion in complexes **1−4** has been directly probed using Cr K-edge XAS. Spectra are presented in Figure 6, and peak energies are listed in Table 5. Remarkably, the lowest energy pre-edge transition of species **1**, **3**, and **4** is seen at very similar energy (5990.5 ± 0.2 eV). Only for **2** a shift
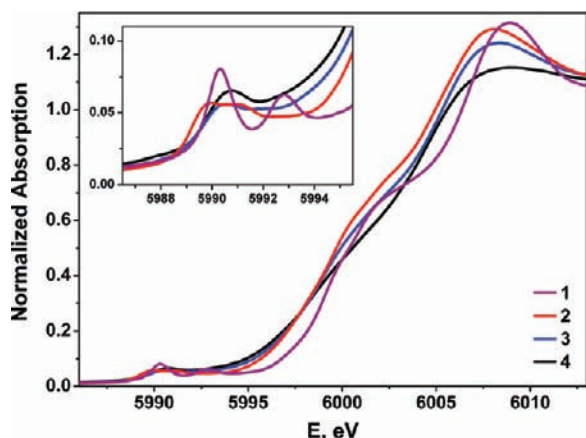
Figure 6. Normalized Cr K-edge XAS of $[Cr(tpy)_2](PF_6)_n$ (n = 3 (**1**, purple), 2 (**2**, red), 1 (**3**, blue), and 0 (**4**, black)). (Inset) Expansion of the pre-edge region.

Table 5. Comparison of Experimentally Determined and Calculated Cr K-Pre-Edge Energies (eV) of Complexes

complex	exptl	calcd	ref
$[Cr^{III}(tpy^0)_2]^{3+}$	5990.3	5990.3	this work
	5992.9	5991.6	
		5994.1	
$[Cr^{III}(tpy^{\bullet})(tpy^0)]^{2+}$	5989.9	5990.0	
	5991.0	5990.9	
$[Cr^{III}(tpy^{\bullet})_2]^{1+}$	5990.4	5990.5	
$[Cr^{III}(tpy^{\bullet\bullet})(tpy^{\bullet})]^0$	5990.7	5990.4	
$trans$-$[Cr^{III}Cl_2(OH_2)_4]Cl$	5990.6		25
	5992.7		
$[Cr^{III}(tacn)_2]Br_3{}^a$	5990.4	5990.4	16
	5991.9	5992.7	
$[Cr^{II}(tacn)_2]Cl_2{}^a$ (S = 2)	5988.7	5988.4	
$[Cr^{III}(CN)_6]^{3-}$	5990.3	5990.2	
$[Cr^{II}(CN)_6]^{4-}$ (S = 1)	5989.2	5989.1	

^{a}tacn =1,4,7-triazacyclononane.

of ~0.6 eV to lower energy is observed. These results are considered to be strong evidence that the former three species in the electron transfer series contain a Cr(III) center. Some other octahedral complexes of Cr(III) exhibit the same low-energy peak at 5990.4 ± 0.2 eV.[16,23,25] On the other hand, it is noted that although **2** displays this pre-edge peak at slightly lower energy (5989.9 eV), the energy does not match that observed in genuine octahedral Cr(II) species (high-spin or low-spin, <5989.2 eV).[16] Therefore, we conclude that the Cr(III) center in **2** is slightly more reduced than in the other complexes and exhibits a small degree of Cr(II) character. In comparison, $[Cr^{III}({}^tbpy^{\bullet})({}^tbpy^0)_2]^{2+}$ shows a pre-edge peak at 5990.1 eV.[16]

Neutral **4** exhibits this low-energy Cr K-pre-edge peak at 5990.7 eV. This requires the two coordinated tpy ligands to contribute a total charge of 3−. This means that a coordinated π radical monoanion $(tpy^{\bullet})^{1-}$ (S = $^1/_2$) and a triplet dianion $(tpy^{\bullet\bullet})^{2-}$ (S = 1) are present in **4**, which would afford, via intramolecular antiferromagnetic coupling of the three ligand-centered spins with the paramagnetic central Cr(III) ion (S_{Cr} = $^3/_2$), a diamagnetic ground state. It is conceivable that the mono- and dianion in **4** are delocalized, generating ligand mixed-valency of class II or even III: $(tpy)^{1.5-}$. The latter

proposal would be in agreement with the crystal structure and theoretical results.

■ **CALCULATIONS**

a. Hypothetical Molecules Containing $(tpy)^{0,1-,2-,3-}$ Ligands. In order to obtain some understanding of the structural changes within a $(tpy^n)^n$ (n = 0, 1−, 2−, 3−) ligand coordinated to a redox-inert metal ion as a function of the ligand charge, we used the B3LYP functional to optimize the geometries of $[Zn^{II}Cl_2(tpy^0)]^0$ (S = 0) (**A**) and the following hypothetical molecules: $[Zn^{II}(tpy^{\bullet})Cl(NH_3)]^0$ (S = $^1/_2$) (**B**), $[Zn^{II}(tpy^{2-})(NH_3)_2]^0$ (S = 0 and 1) (**C**), and $[Al^{III}(tpy^{3-})-(NH_3)_3]^0$ (S = $^1/_2$ and $^3/_2$) (**D**). Complex **A** has been synthesized, and its X-ray structure has been reported.[51] The calculated $C_{py}-C'_{py}$ and C−N bond distances of the respective central and terminal pyridine units of the coordinated tpy ligand in complexes **A**−**D** are collated in Table S3, Supporting Information.

The two calculated $C_{py}-C'_{py}$ distances of $(tpy^n)^n$ (n = 0, 1−, 2−, 3−) decrease linearly with increasing ionic charge (Figure 7) ranging from 1.490 Å in the neutral (tpy^0) to 1.402 Å in the
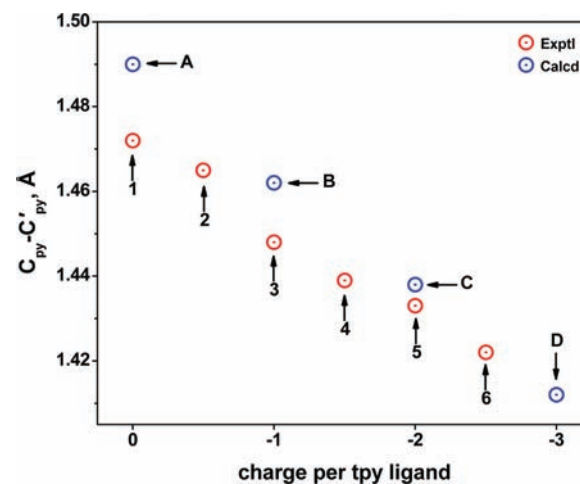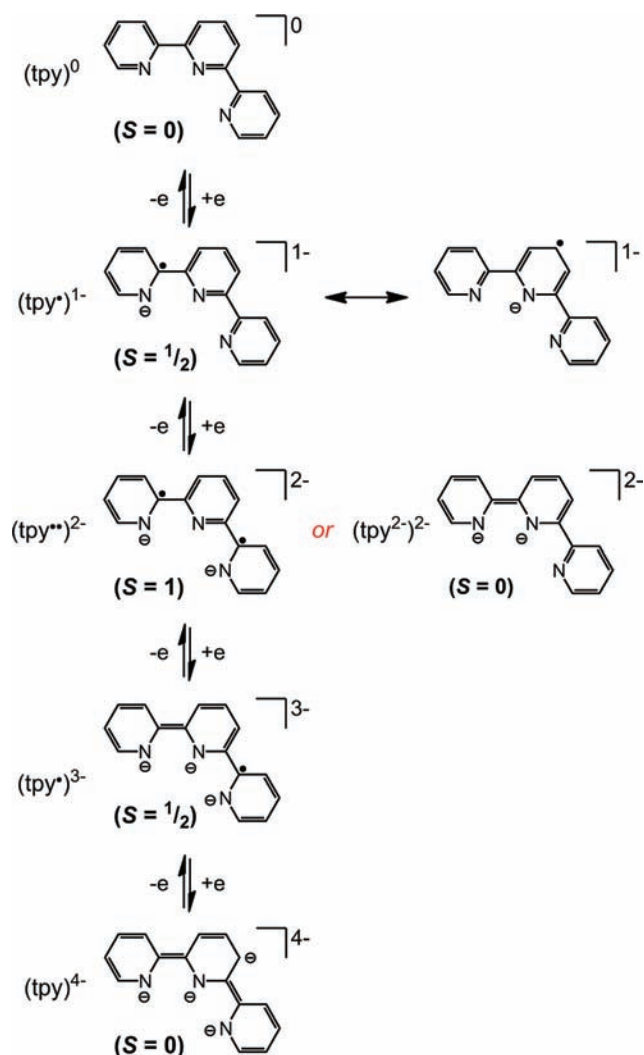

Figure 7. Comparison of the $C_{py}-C'_{py}$ bond lengths (Å) in compounds **1**−**6** (experimental) and compounds **A**−**D** (calculated) showing a monotonic decrease in this bond length for each series.

trianion $(tpy^{3-})^{3-}$ (S = $^1/_2$). In a similar but less pronounced fashion, the two equivalent C−N bond distances of the central pyridine unit lengthen with increasing charge. Even less noticeable is the same effect for the two inequivalent C−N bonds in the two terminal pyridine units.

The dianionic ligand $(tpy^{2-})^{2-}$ in **C** deserves comment. The resonance structures of $(tpy^{2-})^{2-}$ shown in Scheme 1 suggest both diamagnetic and paramagnetic forms. For complex **C**, the singlet diradical ground state (BS(1,1)) was found to be more stable than the triplet excited state by 560 cm^{-1} (J = −280 cm^{-1}).[52] This was also more stable than the closed-shell, spin-restricted Kohn−Sham (RKS) solution by 2.6 kcal mol^{-1} (909 cm^{-1}) The structural changes calculated for the singlet and triplet states are very small (Table S3, Supporting Information); thus, the singlet dianion $(tpy^{2-})^{2-}$ possesses an energetically accessible low-lying excited triplet state, $(tpy^{\bullet\bullet})^{2-}$.

The spin density distribution in paramagnetic **B** (S = $^1/_2$) (Figure 8) displays the presence of a coordinated $(tpy^{\bullet})^{1-}$ π radical ligand, and similarly, the same plot for **D** shows a single unpaired electron on a coordinated $(tpy^{3-})^{3-}$ ligand and no
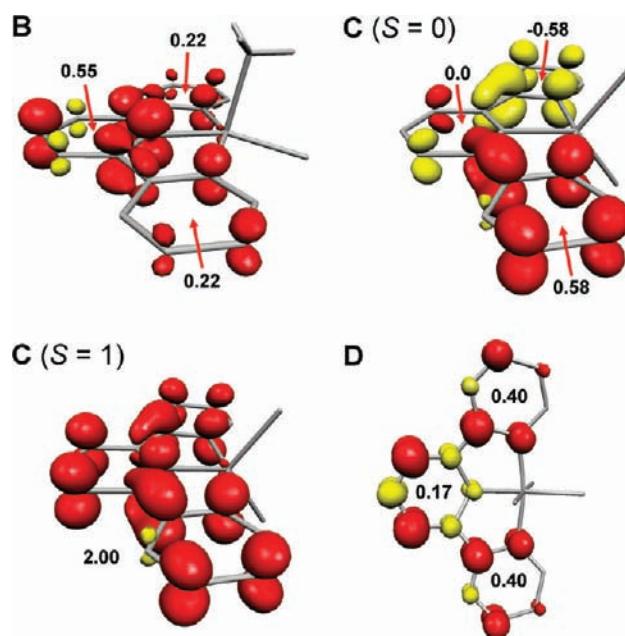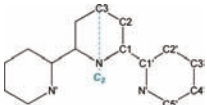
Scheme 1. Resonance Structures of tpy

Figure 8. Calculated Mulliken spin density distribution in **B** ($[Zn^{II}(tpy^•)Cl(NH_3)]^0$; $S = {}^1/_2$), **C** ($[Zn^{II}(tpy^{2-})(NH_3)_2]^0$; $S = 0$ and $S = 1$), and **D** ($[Al^{III}(tpy^{3-})(NH_3)_3]^0$; $S = {}^1/_2$). Hydrogen atoms of the NH_3 ligand in **B** are indicated to differentiate it from the Cl^- ligand.

also best described as $[Co^{II}(tpy^•)(BH_4)]^0$ ($S = 0$): it is a singlet diradical, where a $(tpy^•)^{1-}$ π radical anion is antiferromagnetically coupled to a central low-spin Co(II) ion.

b. Complexes. We optimized the geometry of the $[Cr(tpy)_2]^n$ ($n = 3+$, 2+, 1+, 0, 1−) species and calculated their electronic structures using the B3LYP functional. The optimized coordinates and geometrical details are given in Table 6 and the Supporting Information.

The calculated structure of the trication in **1** agrees very well with the experimental one: C−C and C−N distances are within the ± 0.01 Å range and the Cr−N bond lengths are overestimated by ∼0.03 Å typical of this functional, and two neutral (tpy^0) ligands are identified based on the intraligand bond distances. The MO manifold is marked by three half-filled Cr-centered (>91% Cr) d orbitals representing a $(t_{2g})^3$ set of an octahedral Cr(III) complex: $[Cr^{III}(tpy^0)_2]^{3+}$ ($S = {}^3/_2$).

The broken symmetry BS(3,1) solution and the spin-unrestricted Kohn−Sham (UKS) solution for the dication in **2** were found to be identical. In contrast to the experimental structure with two nonequivalent ligands (one $(tpy^•)^{1-}$ and one (tpy^0)), both tpy ligands were found to be equivalent $((tpy^{0.5-})^{0.5-})$ in the gas phase. The same calculation employing a conductor-like screening model (COSMO)[53] for water afforded a geometry more in keeping with the solid state result with different tpy ligands (Table 6). The central Cr ion again possesses a $(t_{2g})^3$ configuration, and the calculated Mulliken spin density distribution shown in Figure 9 displays α-spin density of ∼2.8 electrons at the Cr(III) ion and β-spin density of −0.8 electrons on the $(tpy^•)^{1-}$ radical anion; (tpy^0) shows a spin of only −0.06. These electrons are intra-molecularly antiferromagnetically coupled, affording the observed $S = 1$ ground state of **2**. The electronic structure of **2** is best described as $[Cr^{III}(tpy^•)(tpy^0)](PF_6)_2$, and we found no computational or experimental evidence for a low-spin Cr(II) ion.[29]

spin density on the $\{Al^{III}(NH_3)_3\}$ moiety. The quartet state of **D** is 18.6 kcal mol^{-1} higher in energy than the doublet state. The calculated Mulliken spin density distribution in **D** is interesting, as it shows that ∼0.4 electrons are located on each of the two terminal pyridine rings whereas only 0.17 of the spin density is located on the central pyridine ring. In contrast, the spin density distribution of the coordinated monoanion $(tpy^•)^{1-}$ ($S = {}^1/_2$) in **B** is localized predominantly on the central pyridine ring (0.55 electrons) as shown experimentally in **2** and its resonance structure in Scheme 1. The spin density distribution generated from the singlet form **C** resulting from the BS(1,1) calculation demonstrates the methodological preference for polarizing the diamagnetic $(tpy)^{2-}$ ligand. Despite the physical irrelevance of BS-DFT-derived spin density for singlet states, it is useful for comparison with other complexes, namely, $[Cr(tpy)_2]^{1-}$ (vide infra).

Gratifyingly, the C−N, C−C, and C_{py}−C'_{py} bond lengths calculated for neutral (tpy^0) in **A** agree nicely with the observed distances in $[Cr^{III}(tpy^0)Cl_3]$ and $[Cr^{III}(tpy^0)_2](ClO_4)_3$.[28,48] It is also worth noting that the calculated geometry of the $(tpy^•)^{1-}$ π radical anion also nicely agrees with experimental data for $[Cr^{III}(tpy^•)(tpy^0)]^{2+}$ and $[Ni^{II}(tpy^•)(CH_3)]^0$.[1,49]

Interestingly, complex $[Co(tpy)(BH_4)]$,[50] which has been structurally characterized by X-ray and neutron diffraction, is

Table 6. Calculated Bond Distances (Å) in $[Cr(tpy)_2]^n$ (n = 3+, 2+, 1+, 0, 1−), 5, and 6

complex	1	2[a]	3	4	$[Cr(tpy)_2]^{1-}$ [b]		5	6
M−N	2.010	1.935	2.028	1.959	1.974	1.985	1.976	2.052	2.034
M−N′	2.085	2.065	2.087	2.074	2.042	2.040	2.062	2.116	2.080
C1−C1′	1.478	1.454	1.478	1.452	1.445	1.427	1.424	1.439	1.430
N−C1	1.352	1.377	1.347	1.380	1.379	1.373	1.381	1.398	1.404
C1−C2	1.398	1.393	1.397	1.393	1.399	1.408	1.402	1.395	1.395
C2−C3	1.401	1.404	1.400	1.404	1.404	1.396	1.400	1.401	1.401
N′−C1′	1.368	1.372	1.363	1.372	1.385	1.394	1.396	1.386	1.392
C1′−C2′	1.395	1.404	1.394	1.406	1.408	1.411	1.413	1.410	1.411
C2′−C3′	1.401	1.391	1.399	1.389	1.386	1.374	1.375	1.385	1.383
C3′−C4′	1.398	1.407	1.396	1.408	1.417	1.422	1.422	1.416	1.420
C4′−C5′	1.396	1.388	1.396	1.388	1.383	1.375	1.379	1.380	1.376
C5′−N′	1.342	1.347	1.338	1.347	1.353	1.348	1.344	1.365	1.373

[a]Bond distances are given for each tpy ligand. [b]Averaged distances in the $(tpy^{2-})^{2-}$ ligand are listed in the second column.
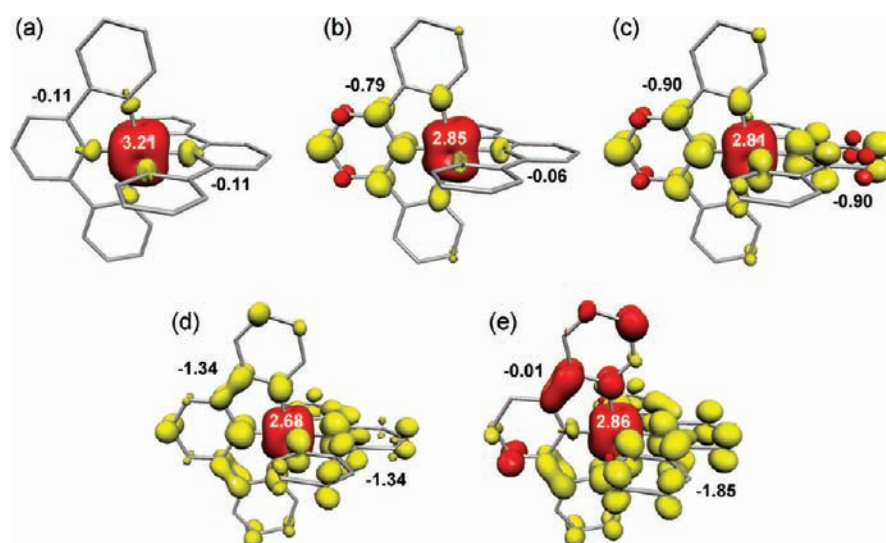

Figure 9. Calculated Mulliken spin density distribution in (a) **1**, (b) **2**, (c) **3**, (d) **4**, and (e) $[Cr(tpy)_2]^{1-}$.

The broken symmetry BS(3,2) and the spin-unrestricted Kohn−Sham solution for the monocation in **3** were also found to be identical; a position not altered with the COSMO model. In excellent agreement with the experimental structure, two identical π radical anions $(tpy^{\bullet})^{1-}$ are identified. The central chromium ion again possesses a $(t_{2g})^3$ electron configuration $(S_{Cr} = {}^3/_2)$. The Mulliken spin density distribution in the monocation shows 2.8 electrons with α-spin at the metal and −0.90 electrons (β-spin) on each $(tpy^{\bullet})^{1-}$ ligand. Thus, the electronic structure of **3** is best described as $[Cr^{III}(tpy^{\bullet})_2](PF_6)$. It is interesting to note that the Mulliken spin density distribution of the $(tpy^{\bullet})^{1-}$ radical anion in both **2** and **3** is predominantly localized on the central pyridine ring of the $\{Cr^{III}(tpy^{\bullet})\}$ moiety; the two outer pyridine rings carry very little spin density. This is in excellent agreement with the observation that the two C−N bonds of this central pyridine ring are observed and calculated to be significantly longer than the corresponding bonds in the outer two. Thus, in the coordinated $(tpy^{\bullet})^{1-}$, the central ring is slightly more dearomatized (electron rich) than the two outer pyridine rings as shown in Scheme 1 and hypothetical **B**.

For the neutral **4**, it was found that the BS(3,3) solution is 18.8 kcal mol^{-1} more stable than the corresponding spin-restricted Kohn−Sham (RKS) solution for a closed-shell molecule. There are two equivalent tpy ligands whose calculated and experimental C−C and C−N bond distances are in excellent agreement. This result is independent of a dielectric continuum. These bonds are intermediate between those of a $(tpy^{\bullet})^{1-}$ π radical monoanion and the triplet diradical $(tpy^{\bullet\bullet})^{2-}$ dianion, indicating that the excess electron is delocalized over both tpy ligands, an $S = {}^3/_2$ $(tpy_2)^{3-}$ unit. Three half-filled orbitals of high Cr d character are observed, indicating the presence of a +III ion with a $(t_{2g})^3$ configuration, where these α-spins (2.68 electrons) are strongly intramolecularly antiferromagnetically coupled to the three unpaired electrons with β-spin (−1.34 electrons per tpy ligand), affording the observed singlet ground state. The calculated coupling constant $J = -1040$ cm^{-1} agrees well with the observation that, in the temperature range 4−290 K, the excited triplet state is not populated. This is in contrast to the $[Cr^{III}({}^tbpy^{\bullet})_3]^0$ ($S = 0$) species,[16] where the $(bpy^{\bullet})^{1-}$ π-radicals are coupled to the Cr(III) center more weakly ($J \approx -477$ cm^{-1};

3727

dx.doi.org/10.1021/ic2027219 | *Inorg. Chem.* 2012, 51, 3718−3732

$J = -599$ cm^{-1}). This is most likely a consequence of the fact that the CrN$_6$ polyhedron in $[Cr^{III}(^1bpy^\bullet)_3]^0$, which is of D_3 symmetry, only has a clear antiferromagnetic exchange pathway between two of the three Cr(III) SOMOs (e and a$_1$ symmetry) and two of the three orbitals derived from the LUMO of each bpy fragment (e and a$_2$ symmetry, see ref 16). On the other hand, in **4**, the D_{2d} molecular symmetry provides a splitting of the three chromium-centered SOMOs into orbitals of e and b$_1$ symmetry, and the splitting of the four orbitals derived from the LUMO and LUMO+1 of each tpy ligand are of e, b$_1$, and a$_2$ symmetry (Figure S17, Supporting Information): all three of the metal-centered SOMOs (e and b$_1$ symmetry) overlap with all three of the ligand-centered SOMOs (also of e and b$_1$ symmetry). The b$_1$ orbital mixes evenly with both ligands, leading to strong superexchange between the formally $(tpy^{\bullet\bullet})^{2-}$ and $(tpy^\bullet)^{1-}$ ligands, delocalizing the excess electron. Interestingly, it was shown computationally for hypothetical $[Zn^{II}(tpy^{2-})(NH_3)_3]^0$ (**C**) that the singlet ground state of the coordinated $(tpy^{2-})^{2-}$ dianion is more stable by 560 cm^{-1} than the triplet state. Apparently it is the excited spin state of doubly reduced (tpy^0) that is present in **4**. Previously, we coined this phenomenon "excited state" coordination,[13,54] which is energetically driven by the strong antiferromagnetic coupling interaction between the metal- and ligand-centered SOMOs, which outweighs the energy cost of exciting the ligand.

The EPR spectrum of chemically generated $[Cr(tpy)_2]^{1-}$ ($S = \frac{1}{2}$) was diagnosed as metal-centered with a weakly axial signal at $g \approx 1.97$. Given the recurring theme for all electron transfer series of this type, that the Cr is invariantly +III, the two tpy ligands must both be dianionic on account of the complex charge. However, the net spin is on the metal, so to the best of our knowledge, we present here the first coordination complex with two identically charged ligands that differ only in spin state: one singlet $(tpy^{2-})^{2-}$ and one triplet $(tpy^{\bullet\bullet})^{2-}$. This electronic structure is realized by BS-DFT calculations. Both the BS(3,2) and the BS(4,3) computations converged to the same solution, namely, that of the latter. This complex arrangement is composed of three α-spins on the Cr(III) ion, two β-spins on the triplet $(tpy^{\bullet\bullet})^{2-}$, and one of each on the singlet $(tpy^{2-})^{2-}$ (Figure 9). This was the same outcome for the (tpy)$^{2-}$ ($S = 0$) ligand in hypothetical **C**, and it must be noted that the apparent polarization of the singlet (tpy)$^{2-}$ ligand as merely one depiction of the spin distribution that has no physical meaning for singlet states (Figure 8). The bound triplet ligand is stabilized by strong antiferromagnetic coupling with two Cr t$_{2g}$ electrons generating two sets of magnetic orbitals with spatial overlaps of S = 0.46 and 0.44 (Figure S18, Supporting Information). The remaining unpaired electron at the metal is insufficient to support a second triplet (tpy)$^{2-}$, so the outcome is a singlet (tpy)$^{2-}$ ligand. By virtue of this arrangement, the point symmetry is lowered to Cs. Each terminal pyridine ring of the singlet (tpy)$^{2-}$ forms a π bonding interaction with the remaining Cr t$_{2g}$ orbital, one with ~50% metal character, whereas the other is predominantly ligand-based (Figure S18, Supporting Information). The α-spin component of the π orbital with 53% Cr content antiferromagnetically couples with the ligand-based β-spin π orbital, forming the third magnetic pair in this complex with overlap S = 0.58. The SOMO is the π^* counterpart with equal contributions of metal and ligand in accordance with the EPR result; the ~52% Cr content is consistent with the small g-anisotropy in the spectrum.

c. Calculated Cr K-Pre-Edge Spectra. A simple TD-DFT approach has been developed for calculation of pre-edge X-ray absorption spectra[55] and successfully utilized in assigning Cr K-edge spectra.[16,23] Due to the limitations in the accurate treatment of excited states in DFT, *absolute* transition energies cannot be obtained by this method. Nevertheless, the *relative* transition energies and the *relative* intensities are, in general, reliably modeled. For a given theoretical method, that is, combination of functional, basis sets, relativistic treatment, and so forth, an empirical correction factor for energy and intensity can be introduced. The specific correction for the calculations presented in this work is 125.34 eV.

The pre-edge region of complexes **1**−**4** shown in the inset of Figure 6 reveals peaks from weak quadrupole-allowed Cr 1s → 3d transitions that gain intensity through symmetry-allowed d−p mixing that bestows significant electric dipole character. The calculated spectra are shown in Figure 10 and display very good
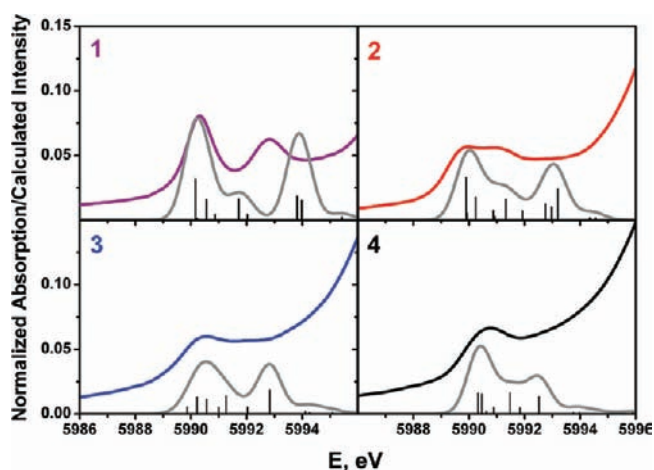

Figure 10. Comparison of the calculated (gray) Cr K-pre-edge with experimental data for **1** (purple), **2** (red), **3** (blue), and **4** (black). Columns depict the calculated transitions; calculated intensity in arbitrary units.

agreement with the experimental values (Table 5). The stick plots in Figures 10 and 11 represent the sum of the dipole and quadrupole contributions to the calculated transition intensities, and the compositions of the acceptor MOs are listed in Table S4, Supporting Information. Despite the low Cr d content of these MOs, the transitions are moderately intense because of a small but crucial contribution from the Cr 4p orbitals (~0.3%). The first two pre-edge peaks in all spectra comprise the 1s → t$_{2g}$(β) and 1s → e$_g$(α) transitions. For octahedral Cr(III) species **1**−**4**, the first pre-edge peak is observed and calculated at 5990.3 ± 0.4 eV, in excellent agreement with the peak at 5990.6 eV observed for *trans*-$[Cr^{III}Cl_2(OH_2)_4]Cl$ and the peak at 5990.4 eV observed for $[Cr^{III}(tacn)_2]^{3+}$ containing the pure σ-donor ligand 1,4,7-triazacyclononane.[16] Genuine octahedral Cr(II) complexes $[Cr^{II}(tacn)_2]^{2+}$ ($S = 2$) and $[Cr^{II}(CN)_6]^{4-}$ ($S = 1$) display this peak at lower energy, 5988.7 and 5989.2 eV, respectively (Table 5).[16] The two transitions comprising the second peak at ~5991.6 eV are the 1s → e$_g$(β) excitation. The third peak at 5994.1 eV comprises the transitions 1s → π^*(tpy). This is shown schematically in Figure 11 for complex **1**. In excellent agreement with experiment, the above calculations clearly show that the central chromium ion in **1**−**4** retains its +III oxidation state irrespective of the overall charge, as described for the
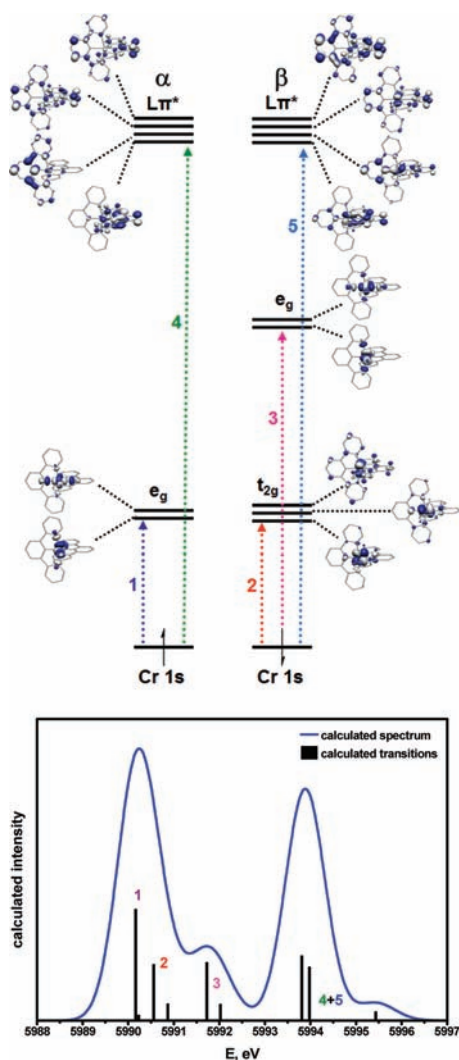
Figure 11. (Top) Qualitative MO scheme presenting the lowest unoccupied orbitals derived from a B3LYP DFT calculation and the five transitions that comprise the calculated pre-edge energy. MO compositions are listed in Table S4, Supporting Information. (Bottom) Simulated Cr K-pre-edge spectrum of **1**. Total calculated intensity (in arbitrary units) represents the sum of the dipole and quadrupole contributions.

corresponding series $[Cr^{III}(bpy)_3]^{3+,2+,1+,0}$ [16] and its analogues.[23,25]

d. Calculated Low-Energy Electronic Transitions. We observed transitions in the IR region of complexes **2**–**4** of sufficient intensity and bandwidth to be considered electronic transitions (Figure 12). Their assignment has been corroborated by TD-DFT calculations. The results are summarized in Table 3, and experimental and calculated spectra are compared in Figure 12.

The observation that (tpy^0) may be reduced by at least two electrons under synthetically relevant conditions to the triplet $(tpy^{••})^{2-}$ ligand in **4** reveals that there are two energetically accessible molecular orbitals (LUMO and LUMO+1, Figure 1). As mentioned above and detailed in Figure 12, the LUMO and LUMO+1 of the two tpy ligands of complexes **3** and **4** combine in D_{2d} symmetry to afford a degenerate set of orbitals (e symmetry) as well as a weakly bonding and antibonding orbital of b_1 and a_2 symmetry, respectively. A central Cr(III) ion of molecular D_{2d} symmetry possesses three SOMOs: two of e

symmetry and one of b_1. The ligand- and metal-centered orbitals of the same symmetry interact weakly, resulting in two bonding and two antibonding orbitals of e symmetry, a bonding and antibonding set of b_1 symmetry, as well as a ligand-centered, nonbonding MO of a_2 symmetry. These orbitals are filled with four ($S = 1$), five ($S = \frac{1}{2}$), and six ($S = 0$) electrons in complexes **2**, **3**, and **4**, respectively, and electronic transitions from the occupied members into the unoccupied members of these orbitals comprise the low-energy electronic transitions observed in their IR and NIR absorption spectra (Figure 12).[56] In **2**, a Jahn–Teller distortion lowers the overall symmetry of this species to C_{2v}, lifting the degeneracy generating two orbitals of b_1 and b_2 symmetry, and the orbitals of b_1 and a_2 symmetry in the D_{2d} point group commute as a_2 in C_{2v} symmetry (where the x and y axes are rotated 45° away from the C_2' axes of the D_{2d} point group). This distortion gives rise to the observed localization of the ligand-centered electron in the X-ray structure of **2**. In the case of **4**, the highest energy ligand-centered SOMO is nondegenerate and incapable of localizing the $(tpy^{••})^{2-}$ ligand, consistent with the structural data (Figure S17, Supporting Information).

Complex **2** shows a peak at 2700 cm^{-1} (calcd 3213 cm^{-1}) that is assigned to the $1b_2(\beta) \rightarrow 1a_2(\beta)$ LLCT excitation (Figure 12). The IVCT band ($1b_2(\beta) \rightarrow 1b_1(\beta)$) is calculated at 522 cm^{-1} with very low intensity and has not been identified experimentally. A second LLCT transition at 9680 cm^{-1} is defined as the $1b_2(\beta) \rightarrow 2a_2(\beta)$ excitation at 8664 cm^{-1} in the computations. Complex **3** possesses two $(tpy^{•})^{1-}$ ligands and exhibits a broad, asymmetric band spanning 4500–5500 cm^{-1}. Two transitions at 4507 and 4513 cm^{-1} are identified in the calculations for this species and defined as excitations from degenerate $1e(\beta)$ into the ligand-based $1b_2(\beta)$ MO (Figure 12). The calculated transitions $1e(\beta) \rightarrow 1a_2(\beta)$ at 9085 and 9089 cm^{-1} agree well with the bands at 8570 and 8930 cm^{-1}, respectively, observed in the electronic absorption spectrum (Figure 3). Finally, **4** is calculated to have transitions associated with excitation from the $1e(\beta)$ and $1b_1(\beta)$ SOMOs into $1a_2(\beta)$ (Figure 12). The IVCT transition is computed at 6422 cm^{-1} and corresponds to the peak at 6680 cm^{-1} in the IR spectrum; the shoulder feature seen at 7210 cm^{-1} in this spectrum presumably accounts for the LLCT excitations calculated at 7120 and 7127 cm^{-1}. The agreement between the calculated and the experimental low-energy electronic transitions of complexes **2**–**4** gives us further confidence in our electronic structure assignments for these species. The results also highlight the energetically low-lying nature of the LUMO and LUMO+1 of (tpy^0) that are responsible for the accessibility of the triplet $(tpy^{••})^{2-}$ ligand that we observed for the first time in **4**.

■ **DISCUSSION**

We have shown that the neutral ligand 2,2′:6′,2″-terpyridine may exist at four distinct oxidation levels, namely, the neutral (tpy^0), the π radical monoanion $(tpy^{•})^{1-}$, the dianion with a singlet $(tpy^{2-})^{2-}$ or a triplet $(tpy^{••})^{2-}$ spin state, and at least, formally, the trianion $(tpy^{3-})^{3-}$ ($S = \frac{1}{2}$). When the two lowest unoccupied molecular orbitals of the neutral (tpy^0) molecule (Figure 1) are filled with electrons in a stepwise manner, small structural changes of the tpy skeleton are observed. For example, the two $C_{py}–C_{py}'$ bond lengths between the three pyridine rings decrease linearly with increasing negative charge, n, $((tpy^n)^n$ ($n = 0, 1-, 2-, 3-$)), from 1.49 Å when $n = 0$ to 1.41 Å when $n = 3-$ (Figure 7). In principle, these changes may

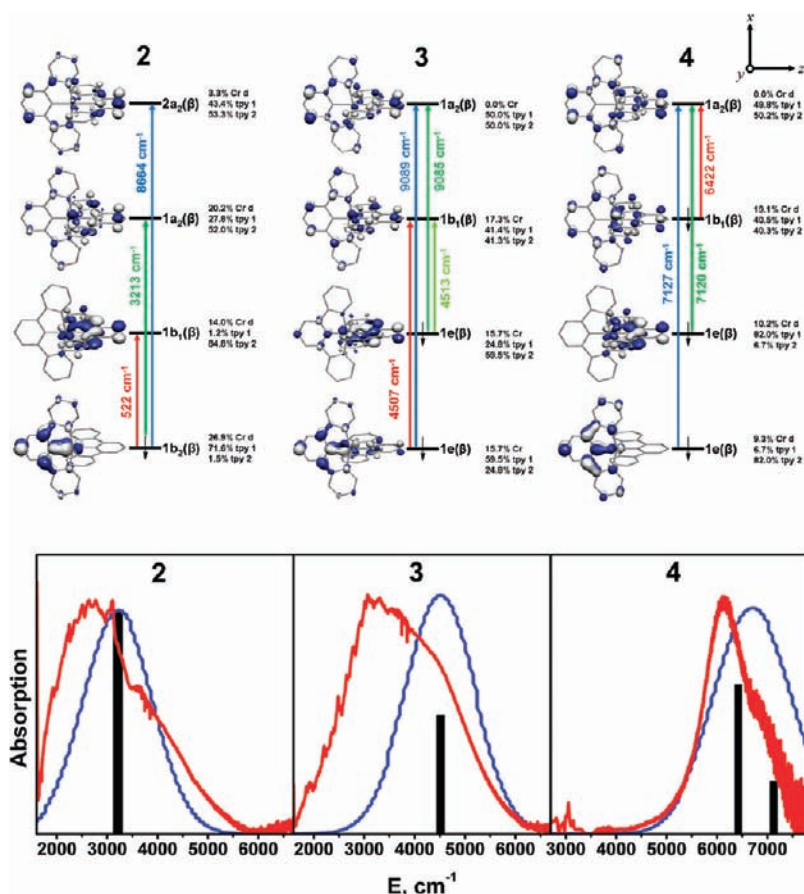**Figure 12.** (Top) Qualitative MO manifolds and calculated electronic low-energy transitions for **2** (annotated with C_{2v} symmetry labels), **3**, and **4** (annotated with D_{2d} symmetry labels). (Bottom) Experimental (IR spectra) and calculated low-energy electronic transitions in complexes **2**–**4**. Red is the experimental spectrum, blue is the calculated spectrum, and black bars are calculated transitions. Vibrational bands observed at lower energies are omitted. Calculated transition shown for **3** contains two excitations of nearly equivalent energy. A 0.2 eV (1613 cm^{-1}) line broadening has been applied to all calculated transitions.

be observed in high-quality X-ray crystallographic structure determinations at cryogenic temperatures. Also, the C−N bonds in all three pyridine rings lengthen with increasing reduction, indicating a stepwise dearomatization. In general, these structural changes are smaller than those observed for the three oxidation levels of bpy: (bpy^0), (bpy$^•$)$^{1-}$, and (bpy^{2-})$^{2-}$ because tpy has a more extensive π system.[16,17]

The hypothetical molecule $[Zn^{II}(tpy^{2-})(NH_3)_2]^0$ (**C**) possesses an $S = 0$ ground state with an excited triplet state ($S = 1$) 560 cm^{-1} above the ground state. The putative trianion (tpy^{3-})$^{3-}$ possesses an $S = \frac{1}{2}$ ground state and has been identified in the hypothetical molecule $[Al^{III}(tpy^{3-})(NH_3)_3]^0$ (**D**). Both the di- and trianion of tpy have not been identified in coordination compounds to date. The neutral diamagnetic complex $[Cr^{III}(tpy^{••})(tpy^{•})]^0$ (**4**) presents an opportunity to study reduced tpy ligands. The ligand mixed-valency in **4** is class III (fully delocalized): the two tpy ligands in each compound are identical in the solid state, and the computed electronic structure of this compound confirms full delocalization of the excess electron over both tpy ligands. Upon moving to heavier metals, the average value of the four C_{py}−C'_{py} bond length is noticeably shorter in **5** and **6** compared to **4** (Figure 5 and Table 4). On the basis of these crystallographic data, we propose that the overall anionic charge of the tpy$_2$ unit in **4**, **5**, and **6** increases from 3− in **4**, to 4− in **5** ($[Mo^{IV}(tpy_2^{4-})]^0$), and finally to 5− in **6** ($[W^V(tpy_2^{5-})]^0$), which implies the presence of (tpy^{3-})$^{3-}$ in **6**, although this interaction is highly covalent (Figure S19, Supporting Information), precluding a strict integer assignment of metal and ligand oxidation levels in **5** and **6**. The tpy oxidation level assignment in complexes **4**–**6** is nicely corroborated by comparing the C_{py}−C'_{py} bond lengths of these compounds with those of the calculated compound $[Zn^{II}Cl_2(tpy^0)]^0$ (**A**) and the hypothetical compounds $[Zn^{II}(tpy^{•})Cl(NH_3)]^0$ (**B**), $[Zn^{II}(tpy^{2-})(NH_3)_2]^0$ (**C**), and $[Al^{III}(tpy^{3-})(NH_3)_3]^0$ (**D**) (Figure 7). We realize that this assignment is spectroscopically (by XAS) and computationally corroborated only for **4** but not to the same degree for **5** and **6**. It is remarkable that the electronic spectra of **4**, **5**, and **6** shown in Figure 3 are so different considering they all possess a singlet ground state; the electronic transitions in the range 25 000− 9000 cm^{-1} have been assigned as predominantly intraligand π^*−π^* in character. This apparently points to the presence of differently charged (tpy$_2$)^n units in **4** ($n = 3-$), **5** ($n = 4-$), and **6** ($n = 5-$). It is also interesting that for **4** the BS(3,3) solution is 18.8 kcal mol^{-1} more stable than the closed-shell RKS solution but for **5** and **6** no BS solution could be found, consistent with the higher covalency observed for second- and third-row transition metals.

The electronic spectra of $[Fe^{II}(tpy^{•})_2]^0$ ($S = 0$)[45] and $[Ru^{II}(tpy^{•})_2]^0$ ($S = 0$)[57] are very similar to that found here for $[Cr^{III}(tpy^{•})_2]^{1+}$ (**3**), where the intraligand $\pi^* \rightarrow \pi^*$ transitions dominate the bands in the range 25 000−11 000 cm^{-1} for the

$(tpy^\bullet)^{1-}$ π radical monoanion. The Cr K-edge spectrum of **3** unambiguously establishes the presence of a central Cr(III) ion. The two π radicals couple strongly intramolecularly to the three unpaired electrons of the Cr(III) ion, yielding an $S = \frac{1}{2}$ ground state that is nicely corroborated by EPR.

Along the same line of argument, the electronic spectrum of the dication in **2**, namely, $[Cr^{III}(tpy^\bullet)(tpy^0)]^{2+}$ ($S = 1$), exhibits, in the range 25 000−9000 cm^{-1}, only intraligand $\pi^* \rightarrow \pi^*$ transitions of the coordinated $(tpy^\bullet)^{1-}$ ligand and an additional electronic transition at 2700 cm^{-1} in the IR. The observed electronic spectrum, Cr pre-edge peak energy, and the structure of the dication rule out its description as $[Cr^{II}(tpy^0)_2]^{2+}$ containing a low-spin Cr(II) ion and two neutral (tpy^0) ligands.[29]

Taking the experimental and DFT computational results together, we assigned the following electronic structures for complexes **1−4**: $[Cr^{III}(tpy^0)_2](PF_6)_3$ ($S = \frac{3}{2}$) for **1**, $[Cr^{III}(tpy^\bullet)(tpy^0)](PF_6)_2$ (localized valencies, $S = 1$) for **2**, $[Cr^{III}(tpy^\bullet)_2](PF_6)$ ($S = \frac{1}{2}$) for **3**, and $[Cr^{III}(tpy^{\bullet\bullet})(tpy^\bullet)]^0$ (delocalized valencies, $S = 0$) for **4**.

The monoanion, $[Cr(tpy)_2]^{1-}$ ($S = \frac{1}{2}$), has the most spectacular electronic arrangement of this electron transfer series. Under highly reducing conditions we recorded its EPR spectrum and show it is consistent with a Cr-centered paramagnetic species. The only electronic structure that is consistent with this observation is $[Cr^{III}(tpy^{2-})(tpy^{\bullet\bullet})]^{1-}$, a coordination complex with the same dianionic ligand but a different spin state. The triplet tpy^{2-} ligand is stabilized by strong antiferromagnetic coupling with the Cr(III) ion; however, the remaining Cr α-spin is not sufficient to support a second excited ligand, so the diamagnetic form binds. To the best of our knowledge, this assembly has never been encountered before, though it can be envisaged that analogous redox-active pincer ligands bound to Cr could produce similar dizygoleptic complexes.

CONCLUSIONS

We have shown that the 2,2′:6′,2″-terpyridine ligand is redox-active and may function as a terdentate ligand in at least four different oxidation levels: (1) the neutral ligand (tpy^0), (2) the monoanionic π radical $(tpy^\bullet)^{1-}$, (3) the dianionic singlet $(tpy^{2-})^{2-}$ or triplet $(tpy^{\bullet\bullet})^{2-}$ species, and (4) possibly even the trianionic doublet π radical $(tpy^{3-})^{3-}$. Moreover, we demonstrated that both singlet and triplet forms of tpy can coexist in the same coordination compound. We tracked the changes in the $C_{py}-C'_{py}$ bond distances and the hallmark low-energy intervalence and ligand-to-ligand transitions in electronic absorption and IR spectra to identify the tpy oxidation level. Complementary XAS and EPR spectroscopic measurements define the metal oxidation state and, where applicable, probe the distribution of spin density. The increasing accuracy and utility of theoretical calculations corroborate the spectroscopic assignment and present an electronic structure description for this electron transfer series. By determining the conditions under which reduced tpy ligands can be accessed, metal−ligand redox interplay presents a new frontier in the design of catalysts utilizing earth-abundant metals.

ASSOCIATED CONTENT

Ⓢ Supporting Information

Crystallographic information files (cif) of complexes **2−6**; temperature dependence of the magnetic moments of **1−6**; EPR spectra of **3** and $[Cr(tpy)_2]^{1-}$; depictions of the crystal structures of **2**, **3**, **5**, and **6**; geometry-optimized coordinates, calculated frontier molecular orbitals, absolute energies of complexes **1−6**, $[Cr(tpy)_2]^{1-}$, **A−D**, and $[Co(tpy)(BH_4)]$, and calculated Cr 3d and 4p contributions to acceptor orbitals. This material is available free of charge via the Internet at http://pubs.acs.org.

AUTHOR INFORMATION

Corresponding Author

*E-mail: sproules@mpi-muelheim.mpg.de (S.S.); wieghardt@mpi-muelheim.mpg.de (K.W.).

Notes

The authors declare no competing financial interest.

ACKNOWLEDGMENTS

REFERENCES

(1) (a) Anderson, T. J.; Jones, G. D.; Vicic, D. A. *J. Am. Chem. Soc.* **2004**, *126*, 8100. (b) Jones, G. D.; McFarland, C.; Anderson, T. J.; Vicic, D. A. *Chem. Commun.* **2005**, 4211.

(2) Jones, G. D.; Martin, J. L.; McFarland, C.; Allen, O. R.; Hall, R. E.; Haley, A. D.; Brandon, R. J.; Konovalova, T.; Desrochers, P. J.; Pulay, P.; Vicic, D. A. *J. Am. Chem. Soc.* **2006**, *128*, 13175.

(3) Ciszewski, J. T.; Mikhaylov, D. Y.; Holin, K. V.; Kadirov, M.; Budnikova, Y. H.; Sinyashin, O.; Vicic, D. A. *Inorg. Chem.* **2011**, *50*, 8630.

(4) Gong, H.; Gagné, M. R. *J. Am. Chem. Soc.* **2008**, *130*, 12177.

(5) Gong, H.; Sinisi, R.; Gagné, M. R. *J. Am. Chem. Soc.* **2007**, *129*, 1908.

(6) Joshi-Pangu, A.; Ganesh, M.; Biscoe, M. R. *Org. Lett.* **2011**, *13*, 1218.

(7) Mikhaylov, D. Y.; Budnikova, Y. H.; Gryaznova, T. V.; Krivolapov, D. V.; Litvinov, I. A.; Vicic, D. A.; Sinyashin, O. G. *J. Organomet. Chem.* **2009**, *694*, 3840.

(8) Prinsell, M. R.; Everson, D. A.; Weix, D. J. *Chem. Commun.* **2010**, *46*, 5743.

(9) Gong, H.; Andrews, R. S.; Zuccarello, J. L.; Lee, S. J.; Gagné, M. R. *Org. Lett.* **2009**, *11*, 879.

(10) Lin, X.; Phillips, D. L. *J. Org. Chem.* **2008**, *73*, 3680.

(11) Chirik, P. J.; Wieghardt, K. *Science* **2010**, *327*, 794.

(12) (a) Bianchini, C.; Giambastiani, G.; Guerrero Rios, I.; Mantovani, G.; Meli, A.; Segarra, A. M. *Coord. Chem. Rev.* **2006**, *250*, 1391. (b) Gibson, V. C.; Redshaw, C.; Solan, G. A. *Chem. Rev.* **2007**, *107*, 1754. (c) Knijnenburg, Q.; Gambarotta, S.; Budzelaar, P. H. M. *Dalton Trans.* **2006**, 5442. (d) Zhu, D.; Thapa, I.; Korobkov, I.; Gambarotta, S.; Budzelaar, P. H. M. *Inorg. Chem.* **2011**, *50*, 9879.

(13) Bart, S. C.; Chłopek, K.; Bill, E.; Bouwkamp, M. W.; Lobkovsky, E.; Neese, F.; Wieghardt, K.; Chirik, P. J. *J. Am. Chem. Soc.* **2006**, *128*, 13901.

(14) (a) de Bruin, B.; Bill, E.; Bothe, E.; Weyhermüller, T.; Wieghardt, K. *Inorg. Chem.* **2000**, *39*, 2936. (b) Enright, D.;

Gambarotta, S.; Yap, G. P. A; Budzelaar, P. H. M. *Angew. Chem., Int. Ed.* **2002**, *41*, 3873. (c) Scott, J.; Gambarotta, S.; Korobkov, I.; Knijnenburg, Q.; de Bruin, B.; Budzelaar, P. H. M. *J. Am. Chem. Soc.* **2005**, *127*, 17204. (d) Scott, J.; Gambarotta, S.; Korobkov, I. *Can. J. Chem.* **2005**, *83*, 279. (e) Bart, S. C.; Lobkovsky, E.; Bill, E.; Wieghardt, K.; Chirik, P. J. *Inorg. Chem.* **2007**, *46*, 7055.

(15) (a) Bock, H.; Lehn, J.-M.; Pauls, J.; Holl, S.; Krenzel, V. *Angew. Chem., Int. Ed.* **1999**, *38*, 952. (b) Chisholm, M. H.; Huffman, J. C.; Rothwell, I. P.; Bradley, P. G.; Kress, N.; Woodruff, W. H. *J. Am. Chem. Soc.* **1981**, *103*, 4945. (c) Echegoyen, L.; DeCian, A.; Fischer, J.; Lehn, J.-M. *Angew. Chem., Int. Ed.* **1991**, *30*, 838. (d) Gore-Randall, E.; Irwin, M.; Denning, M. S.; Giocoechea, J. M. *Inorg. Chem.* **2009**, *48*, 8304.

(16) Scarborough, C. C.; Sproules, S.; Weyhermüller, T.; DeBeer, S.; Wieghardt, K. *Inorg. Chem.* **2011**, *50*, 12446.

(17) Scarborough, C. C.; Wieghardt, K. *Inorg. Chem.* **2011**, *50*, 9773.

(18) Hamacher, C.; Hurkes, N.; Kaiser, A.; Klein, A.; Schüren, A. *Inorg. Chem.* **2009**, *48*, 9947.

(19) Hill, M. G.; Bailey, J. A.; Miskowski, V. M.; Gray, H. B. *Inorg. Chem.* **1996**, *35*, 4585.

(20) Kuehl, C. J.; Da Re, R. E.; Scott, B. L.; Morris, D. E.; John, K. D. *Chem. Commun.* **2003**, 2336.

(21) Throughout this paper we use the abbreviations bpy and tpy in a generic sense: no specific oxidation level is implied. When we intend to assign a specific oxidation level to the 2,2′:6′,2″-terpyridine ligand, we use (tpy^0) for the neutral, diamagnetic ligand, (tpy$^\bullet$)$^{1-}$ for the π radical monoanion, (tpy$^{\bullet\bullet}$)$^{2-}$ for the triplet dianion or (tpy^{2-})$^{2-}$ for its singlet form, and (tpy^{3-})$^{3-}$ for the doublet ($S = {}^1/_2$) trianionic form.

(22) Constable, E. C. *Adv. Inorg. Chem.* **1986**, *30*, 69.

(23) Banerjee, P.; Sproules, S.; Weyhermüller, T.; DeBeer George, S.; Wieghardt, K. *Inorg. Chem.* **2009**, *48*, 5829.

(24) (a) Buchanan, R. M.; Downs, H. H.; Shorthill, W. B.; Pierpont, C. G.; Kessel, S. L.; Hendrickson, D. N. *J. Am. Chem. Soc.* **1978**, *100*, 4318. (b) Buchanan, R. M.; Kessel, S. L.; Downs, H. H.; Pierpont, C. G.; Hendrickson, D. N. *J. Am. Chem. Soc.* **1978**, *100*, 7894. (c) Chun, H.; Verani, C. N.; Chaudhuri, P.; Bothe, E.; Bill, E.; Weyhermüller, T.; Wieghardt, K. *Inorg. Chem.* **2001**, *40*, 4157. (d) Joy, S.; Krämer, T.; Paul, N. D.; Banerjee, P.; McGrady, J. E.; Goswami, S. *Inorg. Chem.* **2011**, *50*, 9993. (e) Sproules, S.; Wieghardt, K. *Coord. Chem. Rev.* **2011**, *255*, 837.

(25) Kapre, R. R.; Bothe, E.; Weyhermüller, T.; DeBeer George, S.; Muresan, N.; Wieghardt, K. *Inorg. Chem.* **2007**, *46*, 7827.

(26) Hughes, M. C.; Macero, D. J. *Inorg. Chem.* **1976**, *15*, 2040.

(27) Herzog, S.; Aul, H. *Z. Chem.* **1966**, *6*, 382.

(28) Wickramasinghe, W. A.; Bird, P. H.; Serpone, N. *Inorg. Chem.* **1982**, *21*, 2694.

(29) We note that the electronic structure of **2** has been incorrectly described as low-spin Cr(II) ([Cr^{II}(tpy^0)$_2$]$^{2+}$, $S = 1$) in all major textbooks of inorganic chemistry: (a) Cotton, F. A.; Wilkinson, G.; Murillo, C. A.; Bochmann, M. *Advanced Inorganic Chemistry*, 6th ed.; J. Wiley & Sons: New York, 1999. (b) Greenwood, N. N.; Earnshaw, A. *Chemistry of the Elements*; Wheaton, A. & Co. Ltd., Exeter: Great Britain, 1988; p 1201. (c) Hollemann, F.; Wiberg, E. *Lehrbuch der Anorganischen Chemie*; deGruyter: Berlin, 1995; p 1455. (d) Larkworthy, L. F.; Nolan, K. B.; O'Brien, P. In *Comprehensive Coordination Chemistry*; Wilkinson, G., Gillard, R. D., McCleverty, J. A., Eds.; Pergamon Press: New York, 1987; Vol. 3, p 712.

(30) du Bois, D. W.; Iwamoto, R. T.; Kleinberg, J. *Inorg. Chem.* **1969**, *8*, 815.

(31) Behrens, H.; Anders, U. *Z. Naturforsch., B: Chem. Sci.* **1964**, *19*, 767.

(32) Hanson, G. R.; Gates, K. E.; Noble, C. J.; Griffin, M.; Mitchell, A.; Benson, S. *J. Inorg. Biochem.* **2004**, *98*, 903.

(33) Kapre, R. R.; Ray, K.; Sylvestre, I.; Weyhermüller, T.; DeBeer George, S.; Neese, F.; Wieghardt, K. *Inorg. Chem.* **2006**, *45*, 3499.

(34) Neese, F. *Orca, an Ab Initio, Density Functional and Semiempirical Electronic Structure Program Package*, version 2.8; Universität Bonn: Bonn, Germany, 2010.

(35) (a) Becke, A. D. *J. Chem. Phys.* **1993**, *98*, 5648. (b) Lee, C. T.; Yang, W. T.; Parr, R. G. *Phys. Rev. B* **1988**, *37*, 785.

(36) (a) Grimme, S. *J. Comput. Chem.* **2004**, *25*, 1463. (b) Grimme, S. *J. Comput. Chem.* **2006**, *27*, 1787. (c) Grimme, S.; Antony, J.; Ehrlich, S.; Krieg, H. *J. Chem. Phys.* **2010**, *132*, i54104.

(37) (a) van Lenthe, E.; Baerends, E. J.; Snijders, J. G. *J. Chem. Phys.* **1993**, *99*, 4597. (b) van Lenthe, E.; Baerends, E. J.; Snijders, J. G. *J. Chem. Phys.* **1994**, *101*, 9783. (c) van Wüllen, C. J. *J. Chem. Phys.* **1998**, *109*, 392.

(38) Pantazis, D. A.; Chen, X. Y.; Landis, C. R.; Neese, F. *J. Chem. Theory Comput.* **2008**, *4*, 908.

(39) Sheldrick, G. M. *SADABS, Bruker-Siemens Area Detector Absorption and Other Corrections*, Version 2006/1; Universität Göttingen: Göttingen, Germany, 2006.

(40) *ShelXTL 6.14*; Bruker AXS Inc., Madison, WI, 2003.

(41) Sheldrick, G. M. *ShelXL97*; Universität Göttingen: Göttingen, Germany, 1997.

(42) Flack, H. *Acta Crystallogr.* **1983**, *A39*, 876.

(43) Behrens, H.; Meyer, K.; Müller, A. *Z. Naturforsch., B: Chem. Sci.* **1965**, *20*, 74.

(44) Casellato, U.; Graziani, R.; Bonomo, R. P.; Di Bilio, A. J. *J. Chem. Soc., Dalton Trans.* **1991**, 23.

(45) Braterman, P. S.; Song, J. L.; Peacock, R. D. *Inorg. Chem.* **1992**, *31*, 555.

(46) Nakamura, K. *Bull. Chem. Soc. Jpn.* **1971**, *45*, 1943.

(47) (a) Heath, G. A.; Yellowlees, L. J.; Braterman, P. S. *J. Chem. Soc., Chem. Commun.* **1981**, 287. (b) Heath, G. A.; Yellowlees, L. J.; Braterman, P. S. *Chem. Phys. Lett.* **1982**, *92*, 646.

(48) Cloete, N.; Visser, H. G.; Roodt, A. *Acta Crystallogr.* **2007**, *E63*, m45.

(49) Hamacher, C.; Hurkes, N.; Kaiser, A.; Klein, A. *Z. Anorg. Allg. Chem.* **2007**, *633*, 2711.

(50) Corey, E. J.; Cooper, N. J.; Canning, W. M.; Lipscomb, W. N.; Koetzle, T. F. *Inorg. Chem.* **1982**, *21*, 192.

(51) (a) Dumitru, F.; Petit, E.; van der Lee, A.; Barboiu, M. *Eur. J. Inorg. Chem.* **2005**, 4255. (b) Vlasse, M.; Rojo, T.; Beltran-Porter, D. *Acta Crystallogr.* **1983**, *C39*, 560.

(52) (a) Soda, T.; Kitagawa, Y.; Onishi, T.; Takano, Y.; Shigeta, Y.; Nagao, H.; Yoshioka, Y.; Yamaguchi, K. *Chem. Phys. Lett.* **2000**, *319*, 223. (b) Yamaguchi, K.; Takahara, Y.; Fueno, T. In *Applied Quantum Chemistry*; Smith, V. H., Ed.; Riedel: Dordrecht, The Netherlands, 1986.

(53) Klamt, A.; Schüürmann, G. *J. Chem. Soc., Perkin Trans. 2* **1993**, 799.

(54) Ghosh, P.; Bill, E.; Weyhermüller, T.; Neese, F.; Wieghardt, K. *J. Am. Chem. Soc.* **2003**, *125*, 1293.

(55) (a) Berry, J. F.; DeBeer George, S.; Neese, F. *Phys. Chem. Chem. Phys.* **2008**, *10*, 4361. (b) DeBeer George, S.; Petrenko, T.; Neese, F. *J. Phys. Chem. A* **2008**, *112*, 12936. (c) DeBeer George, S.; Petrenko, T.; Neese, F. *Inorg. Chim. Acta* **2008**, *361*, 965. (d) DeBeer George, S.; Neese, F. *Inorg. Chem.* **2010**, *49*, 1849.

(56) The weakly interacting nature of these orbitals results in a multiconfigurational ground state for complexes **2−4**, and we approximated the configuration interaction using BS DFT.

(57) Berger, R. M.; McMillin, D. R. *Inorg. Chem.* **1988**, *27*, 4245.